ISSN 8755-6839

SCIENCE OF **TSUNAMI HAZARDS**

Journal of Tsunami Society International

Volume 39 **Number 3** **2020**

DEVELOPMENT OF EARTHQUAKE AND TSUNAMI EARLY WARNING APPLICATION BASED ON ANDROID **183**

Madlazim[1], Supriyanto Rohadi[2], Soerja Koesuma[3], Ella Meilianda[4]

[1] State University of Surabaya, Surabaya 60213, ***INDONESIA***
[2]Meteorology Climatology and Geophysics Council, DKI Jakarta 10720, ***INDONESIA***
[3]Sebelas Maret University, Solo 57126, ***INDONESIA***
[4] Syiah Kuala University, Aceh 23111, ***INDONESIA***

WWW.TSUNAMISOCIETY.ORG

TSUNAMI SOCIETY INTERNATIONAL, 1741 Ala Moana Blvd. #70, Honolulu, HI 96815, USA.

SCIENCE OF TSUNAMI HAZARDS is a CERTIFIED OPEN ACCESS Journal included in the prestigious international academic journal database DOAJ, maintained by the University of Lund in Sweden with the support of the European Union. SCIENCE OF TSUNAMI HAZARDS is also preserved, archived and disseminated by the National Library, The Hague, NETHERLANDS, the Library of Congress, Washington D.C., USA, the Electronic Library of Los Alamos, National Laboratory, New Mexico, USA, the EBSCO Publishing databases and ELSEVIER Publishing in Amsterdam. The vast dissemination gives the journal additional global exposure and readership in 90% of the academic institutions worldwide, including nation-wide access to databases in more than 70 countries.

OBJECTIVE: Tsunami Society International publishes this interdisciplinary journal to increase and disseminate knowledge about tsunamis and their hazards.

DISCLAIMER: Although the articles in SCIENCE OF TSUNAMI HAZARDS have been technically reviewed by peers, Tsunami Society International is not responsible for the veracity of any statement, opinion or consequences.

Submit manuscripts of research papers, notes or letters to the Editor. If a research paper is accepted for publication the author(s) must submit a scan-ready manuscript, a Doc, TeX or a PDF file in the journal format. Issues of the journal are published electronically in PDF format. There is a minimal publication fee for authors

who are members of Tsunami Society International for three years and slightly higher for non-members. Tsunami Society International members are notified by e-mail when a new issue is available. Permission to use figures, tables and brief excerpts from this journal in scientific and educational works is granted provided that the source is acknowledged.

Recent and all past journal issues are available at: http://www.TsunamiSociety.org CD-ROMs of past volumes may be purchased by contacting Tsunami Society International at postmaster@tsunamisociety.org Issues of the journal from 1982 thru 2005 are also available in PDF format at the U.S. Los Alamos National Laboratory Library http://epubs.lanl.gov/tsunami/

WWW.TSUNAMISOCIETY.ORG

ISSN 8755-6839

SCIENCE OF **TSUNAMI HAZARDS**

Journal of Tsunami Society International

Volume 39 **Number 3** **2020**

SCOURING ON BOULDER BED BEHIND A SEAWALL DUE TO TSUNAMI

Warniyati[1,3], Radianta Triatmadja[2*], Nur Yuwono[2]

[1]Doctoral Student at Department of Civil and Environmental Engineering Universitas Gadjah Mada, Yogyakarta, Indonesia
[2]Department of Civil and Environmental Engineering Universitas Gadjah Mada, Yogyakarta, Indonesia
[3]Department of Civil Engineering, Engineering Faculty, Universitas Pattimura, Ambon, Indonesia
*Corresponding author: radianta@ugm.ac.id

ABSTRACT

Based on post-tsunami surveys following the Japan Tsunami 2011, the most prominent seawall damage was due to scours that was formed behind the seawall. The downstream of a seawall is an essential part of the seawall stability which must be securely protected from the tsunami overflow in order to maintain seawall stability. The scouring process on boulder bed behind the seawall and the method to reduce the scour was investigated in a laboratory experiment. The scouring process and scour depth are assumed to be closely related with the tsunami hydrograph. Hence, the tsunami hydrograph was also modelled to imitate an existing reported tsunami hydrograph. The results showed that both the maximum scour depth and scour length are increased with the length of tsunami overflow or the hydrograph. The bed material behind the seawall was transported downstream. The transport of boulder can be blocked by a set of vertical screens installed in between the boulder bed. This method is found to be effective in reducing both the scour depth and scour length. The reduction of maximum scour depths are approximately 50%, 43%, and 34% for dimensionless screen distance of 5.33, 6.67, and 8.0, respectively, while the scours length for all various screen distance is reduced for about 25 %. Other than that, it is important to note that the scour depth exactly behind the seawall reduced significantly. This signify that, the screen also effective in keeping in place the bed material that directly support the seawall from sliding force and turning moment and thus secures the stability of the seawall.

Keywords: *tsunami, overflow, scour, screen, mitigation*

Vol 39 No. 3, page 124 (2020)

1 INTRODUCTION

Tsunami is one of the most unpredictable natural disasters that may destroy many structures in coastal area. When a tsunami reaches a beach, it slows down but increases in height due to the reduce water depth (Triatmadja 2010). The run-up of a tsunami in land with extreme energy may severely destroy the inundated land area. A seawall may be constructed to protect the land area from the tsunami attack, such as in the eastern Japan coastal area. The seawall was constructed to protect the essential coastal land and facilities from big waves including typhoons, storm surges, and tsunami that frequently occurred (Fraser et al. 2013).

A tsunami occured on 11 of March 2011 in east Japan that destroyed significant amount of coastal defense in the Japan eastern coast. The demolition of the seawall that was designed as tsunami protection lead to even greater destruction. Based on the many post-tsunami field surveys, there were many destroying patterns of the seawall (Ishikawa et al. 2011, Kato et al. 2012, Mikami, et al. 2012, Suppasri et al. 2013, Sato and Okuma 2014, Jayaratne et al. 2016). The most prominent seawall damage was due to scour that was formed behind the seawall (Kato et al. 2012, Yeh et al. 2013). The tsunami overflowed the seawalls and destroyed many parts of the seawalls. The overflow induced high-speed jet flow behind the seawall and scoured the seawall foundation. Such scour may endanger the seawall stability (Triatmadja et al. 2011, Kato et al. 2012, Suppasri et al. 2013, Jayaratne et al. 2016). When the seawall collapsed due to instability, tsunami could wash out the land and create disaster just like a dam break disaster.

Researches on the countermeasure of scour behind a seawall have been conducted using both physical modeling and numerical modeling. Some of the results are as follows. The tsunami energy can be broken by applying an artificial trench behind the seawall to reduce the scour depth (Tsujimoto et al. 2014). Toe protection can be applied behind the seawall to change the flow direction at the landing point to be horizontal and upward in order to horizontally expand the scour and reduce the scour depth (Mitobe et al. 2014). In the case of a breakwater, a concrete block namely Supleo Frame can be applied behind the seawall as environmentally friendly protection from the scour due to tsunami overflow (Matsushita 2012, Yoshizuka et al. 2018). A horizontal plate was proposed as a method to reduce scour depth due to tsunami overflow behind a breakwater (Sulianto et al. 2014).

Based on the above researches, it is apparent that the downstream of a seawall is an essential part of seawall which must be protected from the tsunami overflow in order to maintain its stability. A heavy material configuration may be used as a protective material of seawall downstream due to the tsunami overflow, although in an extreme condition, scour may still occur. The effort to reduce the scour at the toe protection of seawall should be considered. Warniyati et al. 2019 studied the effectiveness of vertical screen installation within the boulder bed behind a seawall. The results indicates that such screen was capable of reducing the scour depth. This paper explains the mechanism and characteristics of scouring behind the seawall related to tsunami hydrograph. The effects of various screen installations in reducing the scour are also explained.

2 THEORETICAL BACKGROUND

When a water jet impinging on granular bed in a certain jet velocity, the jet energy starts to scour the bed to form a hole. Under a continuous action of the jet, the scour is getting deeper until it reaches a dynamic equilibrium (Gioia and Bombardelli 2005). The equilibrium scour is reached when the rate of scouring comes to zero (Bormann and Julien 1991). On the scour below a vertical drop, the equilibrium scour depth increase with increasing densimetric Froude number, while the increase of diameter and tailwater reduce the scour depth (Dey and Raikar 2007). In the scouring process due to tsunami overflow, the initial density of granular material has a significant effect. The higher is the initial density, the deeper is the maximum scour (Wang et al. 2016). Wang et al. 2016 also found that the overflow height also gives a significant effect on the maximum scour depth and that the scour depth is proportional to the overflow height.

The downstream scour of a seawall due to tsunami overflow are related to the following essential parameters where the boulder material was modelled using gravel material:

1. Overflow jet parameter (water densisty ρ, overflow height h_o, overflow time T_i)
2. Building parameter (seawall height h_b)
3. Gravel material parameter (diameter D_m, spesific gravity ρ_m, distance between screen L_c)

According to the above parameters, general expression representing the scour depth and scour length may be formulated as in Equation 1.

$$\emptyset = f(\rho, h_o, T_i, h_b, D_m, \rho_m, L_c) \tag{1}$$

Using dimensional analysis, the nondimensional parameters of scour depth and scour length are given in Equation 2.

$$\frac{d_s}{h_b}, \frac{L_s}{h_b} = f\left(\frac{L_c}{\Delta\, D_m}, T_i \sqrt{g h_d}\right) \tag{2}$$

where d_s is the maximum scour depth, L_s is the maximum scour length, $\Delta = (\rho_m - \rho)/\rho$ is the relative submerged particle, and $h_d = h_b + h_o$ is the initial head of the jet. With the above parameters, an empirical formula can be found through experimental works in the laboratory.

3 EXPERIMENTAL METHODS

3.1 Experimental Facilities

The experiment was conducted at the Hydraulics Laboratory of Civil and Environmental Engineering, Gadjah Mada University. The experimental facility consists of three parts. The first part is an overhead tank to store water that is equipped with a pipe network. The second part is a short flume to conduct the model test. The dimension of the flume is 9.2 m

long, 0.8 m wide and 2 m high. The last part is a collecting tank to store the tsunami run-up water. In the pipe network, a gate with an electronic controller was installed to adjust the discharge of water from the overhead tank into the flume. The electronic controller can be programmed and operated at a certain speed and time delay to open or close the gate valve that makes the water discharge from the reservoir highly repeatable. In the short flume, a glass panel was provided at one side of the flume to observe the tsunami flow, its interaction with the seawall model, and the scouring process. In the collecting tank, a centrifugal pump was installed to return the water to the overhead tank before the model test is started. The photograph of tsunami generation facilities is shown in Figure 1. The design process of the facilities is available in Warniyati et al. (2019)

Figure 1. Photograph of tsunami generation facilities.

3.2 Bed Material Setup

A seawall model was placed in the middle of the flume. Gravel was placed behind the seawall model to simulate the boulder bed. The seawall model height at the upstream (h_s) was 0.16 m, the movable bed was 0.31 m below the seawall crest. In this case, the seawall height (h_b) is 0.31 m. The gravel material of (D_m) 0.025 m in diameter with density (ρ_m) of 2,500 kg/m^3 and was randomly placed at the downstream of the seawall. The schematic symbol of the flow and scour dimension in this research is shown in Figure 2.

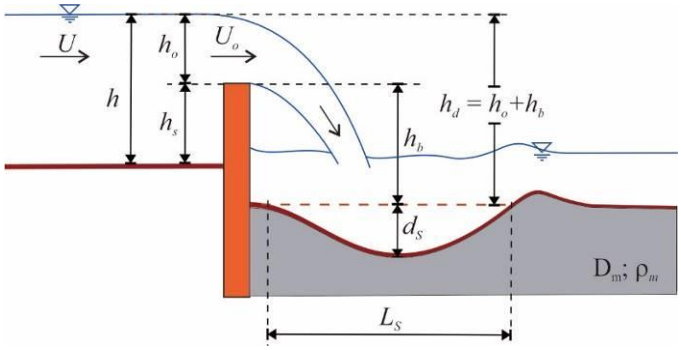

Figure 2. Schematic of symbol

The scouring tests were conducted in two scenarios. In the first scenario, the gravel was loose and was placed randomly behind the seawall. The second scenario was conducted to mitigate or reduce the scour. A set of wire meshes was installed vertically and parallel to the seawall along the movable bed part as screens. The wire meshes model were 0.3 m deep below the bed surface and were installed at a certain distance (L_c) along the movable bed starting exactly behind the seawall. The size of the screen was slightly less than the gravel to ensure that no gravel could pass through the screen. The schematic of the bed material and screen installation is shown in Figure 3.

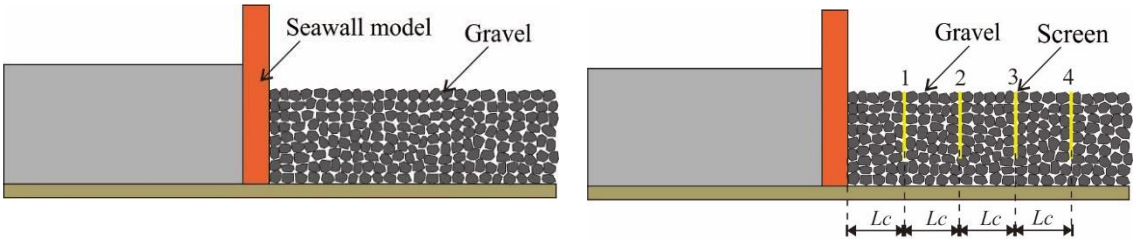

(a) Scenario 1 (without screen) (b) Scenario 2 (with screen)

Figure 3. Schematic of the bed material and screen installation

3.3 Tsunami Generation and Scouring Test

The simulation of tsunami and scour behind of a seawall is explained below referring to Figure 4. Before starting the simulation, the overhead tank was filled with water. By opening the gate valve at the pipe, volume of water was released from the reservoir into the flume. The lower tank's water elevation was maintained at the same level as the elevated fixed bed part before the simulation was started. The lower tank thus represented the sea while the fixed bed represented the land. The water level in the flume was increasing during the opening of the gate valve similar to the tsunami that arrived in land and was stopped by a seawall. After sometime water start overflowing the seawall when the water level is higher than the crest of the seawall model. The overflow continued depending on the tsunami hydrograph that was controlled by using the gate valve. Finally, the hydrograph decreased and then diminished representing the tsunami overflow hydrograph when the valve started closing. The generation of tsunami hydrograph is explained as follows.

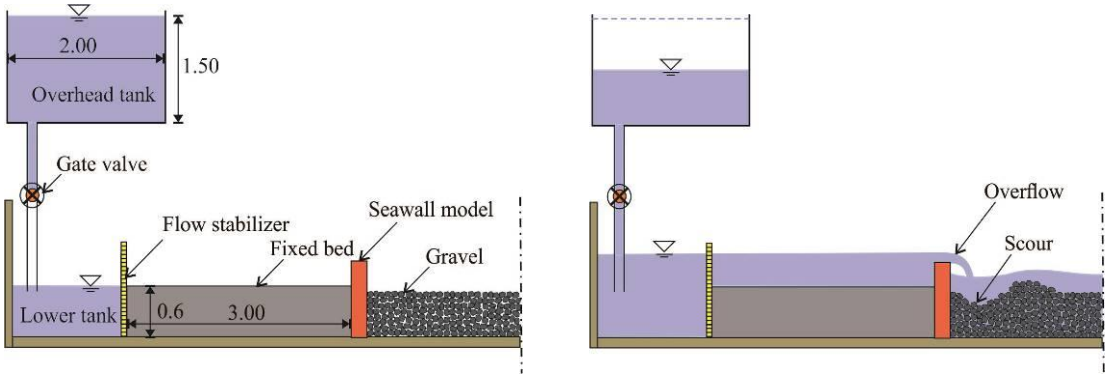

(a) before the simulation started (b) during the simulation

Figure 4. Schematic of tsunami generation and simulation of scouring (unit in meter)

Many scenarios of flow discharges to generate tsunamis were applied. The release of water was controlled by adjusting the speed of opening, the percentage of opening, the delay before the gate was closed, and the speed of closing. The overflow height (h_o) was recorded during the simulation. The tsunami overflow was represented by a tsunami hydrograph, which is the relation of time and tsunami overflow. The tsunami hydrograph was similar to the historical tsunami hydrograph observed during the Japan tsunami in 2011 by Fritz et al. (2012). The tsunami hydrograph in Figure 5 was applied in the simulation of the scouring process. In the tsunami hydrograph, *Ti* is the time duration from the start of the overflow to the inflection point. After that point, the overflow became small and reduced slowly with time. During the tsunami overflow, the inflection point was the most significant part of the tsunami attack on the seawall. Therefore, it is used to specify the tsunami hydrograph. The method to define the inflection point is described in Warniyati et al. (2019).

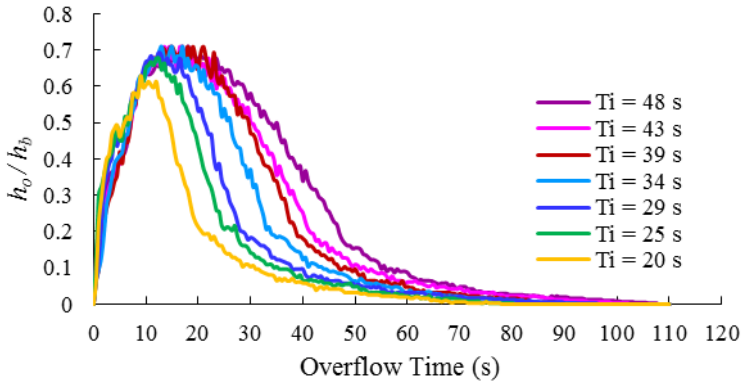

Figure 5. Overflow tsunami hydrograph

4 RESULTS AND DISCUSSION

4.1 Scour at Downstream of a Seawall

Scour behind a seawall started when the overflow jet started to remove the gravel material from the original position and dragged them downstream. When the overflow increased, the scour depth and width increased until a certain condition where the overflow could not scour the gravel bed any further. When the overflow significantly reduced, the overflow jet position shifted upstream and become closer to the seawall. Hence the gravel near the rear wall of the seawall were dragged into the scour that has been previously created (Warniyati et al. 2019). This mechanism resulted in deeper scour near the seawall which was not good in term of seawall stability.

The scouring process during the simulation can be explained based on the relation between tsunami hydrograph and the scour depth in Figure 6. At small overflow discharge (approximately after 2 second of overflow where h_o/h_b =0.2, the jet force could not move the gravel. As can be seen the value of d_s/h_b =0.0. At a certain overflow discharge h_o/h_b = 0.4, the jet force started to move the gravel and scoured the bed. The scour depth increased with the increasing overflow until the condition where the overflow hydrograph reached its

maximum where the jet force and the scour depth reached its balance condition. Such condition was also affected by the increasing tail-water and water cushion above the scour hole. It can be seen in Figure 6, that the longer was the peak of the hydrograph, the longer was the constant (slightly fluctuating) scour depth. When the overflow decreased, the scour depth was reduced because the overflow jet dragged the gravel that were closer to the seawall into the scour hole. Hence the scour depth near the seawall increased in a relatively short time while the maximum scour depth was slightly reduced due to the incoming gravel material from the area next to the sea wall. The final scour depth was reached after the overflow hydrographs almost reached the inflection point. After the point of inflection, the jet force was unable to scour the bed and the scouring process stop. It can be inferred that the scouring process depends on the tsunami hydrograph.

The scouring process behind a seawall due to tsunami overflow is different from the scouring process behind or downstream of a river structure caused by a continuous flow such as weir (Dargahi 2003, Adduce and La Rocca 2006, Dey and Raikar 2007, Guan et al. 2019). The tsunami overflow occurred in a relatively short time and hence, the tsunami hydrograph affected the scouring process. The scouring process in this research is different from the previous researches on tsunami overflow that was conducted by Kato et al. (2012), Tsujimoto (2014), and Wang et al. (2016). The tsunami generation in those researches were using a pump system with continuous and constant flow discharge. Therefore, the application of the tsunami hydrograph in tsunami overflow and the scour process is more realistic when dealing with tsunami event.

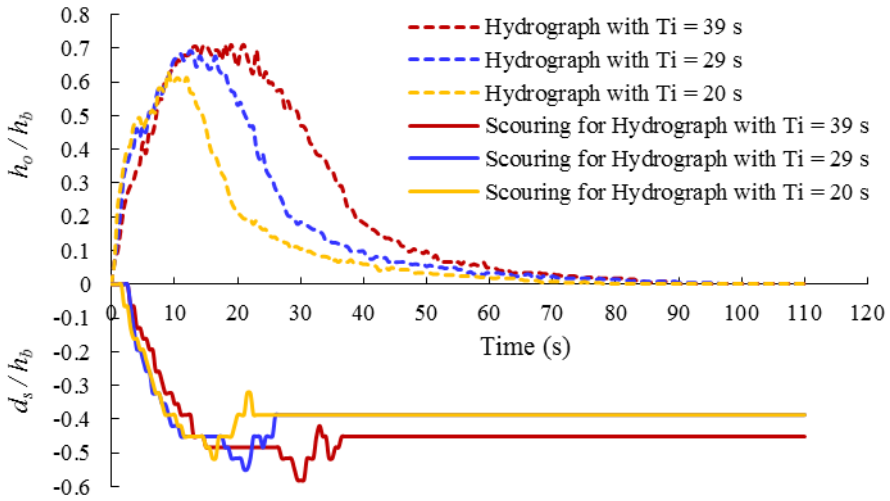

Figure 6. Relation of tsunami overflow and scour depth

4.2 Reduction of Scour Depth by Vertical Screens

It was observed during the experiment that, the jet flow initially created small scour hole in the movable gravel bed. The flow trasported the granular material downstream away from the scour hole and subsequently the jet force created deeper and large scour hole.

As the hole become larger and deeper, the turbulent flow in the scour hole should be able to lift the bed material from a deeper location in order to deepen the scour and move the bed material away. This was possible when the width of the scour was relatively large thus, creating milder slope of the scour where lifting the bed material was easier for the jet flow. Installing the screen limited the possibility of widening the scour hole and hence limited the possibility of the jet to create milder slope and deeper scour hole. The scouring process in both loose material (Case 1) and with screen installation (Case 2) are presented in Figure 7.

In Case 1, the gravel was transported downstream without restriction and were easily washed out downstream. Therefore, the scour increased as long as the jet force was able to lift the bed material. When the scour reached the maximum depth, the jet turbulence continued to drag the bed material downstream hence, the scour area was enlarged to reach the maximum scour length. In Case 2, the transport of the bed material was blocked by the screen. The gravel could only be dragged away by the flow when they were lifted above the top of the screen. This condition limited the scour depth since it was more difficult to lift the bed material within significantly less space (in between two screens) as the scour getting deeper. It was observed during the simulation that screen positions number 2, number 3 and number 4 effectively blocked the transport of the bed material.

As mentioned previously, when the overflow was finally reduced at the end of tsunami hydrograph, the overflow jet scoured the bed close to the seawall and the bed material were deposited in the scour hole that was previously created. In Case 1, the deeper scour adjacent to the seawall may endanger the stability of the seawall as can be seen in Figure 7 (left) at time 25 s. It may create a critical condition for the seawall stability. In the Case 2, the bed material were blocked by the screen at position number 1. The final scour nearby the seawall in Case 2 was almost negligible. Therefore, the seawall stability was maintained (see Figure 7 right).

Both maximum scour and final scour for various scenarios of the bed material arrangement are presented in Figure 8. In the Case 2, the screen installation was applied in three different distances with nondimensional distances ($L_c/\Delta D_m$) were 5.33, 6.67, and 8.0. The screens were installed along the movable bed in the area where the maximum scour length was formed during the experiment with no screen installed. It was clearly seen that the installation of the screens reduced both the scour depth and the scour length.

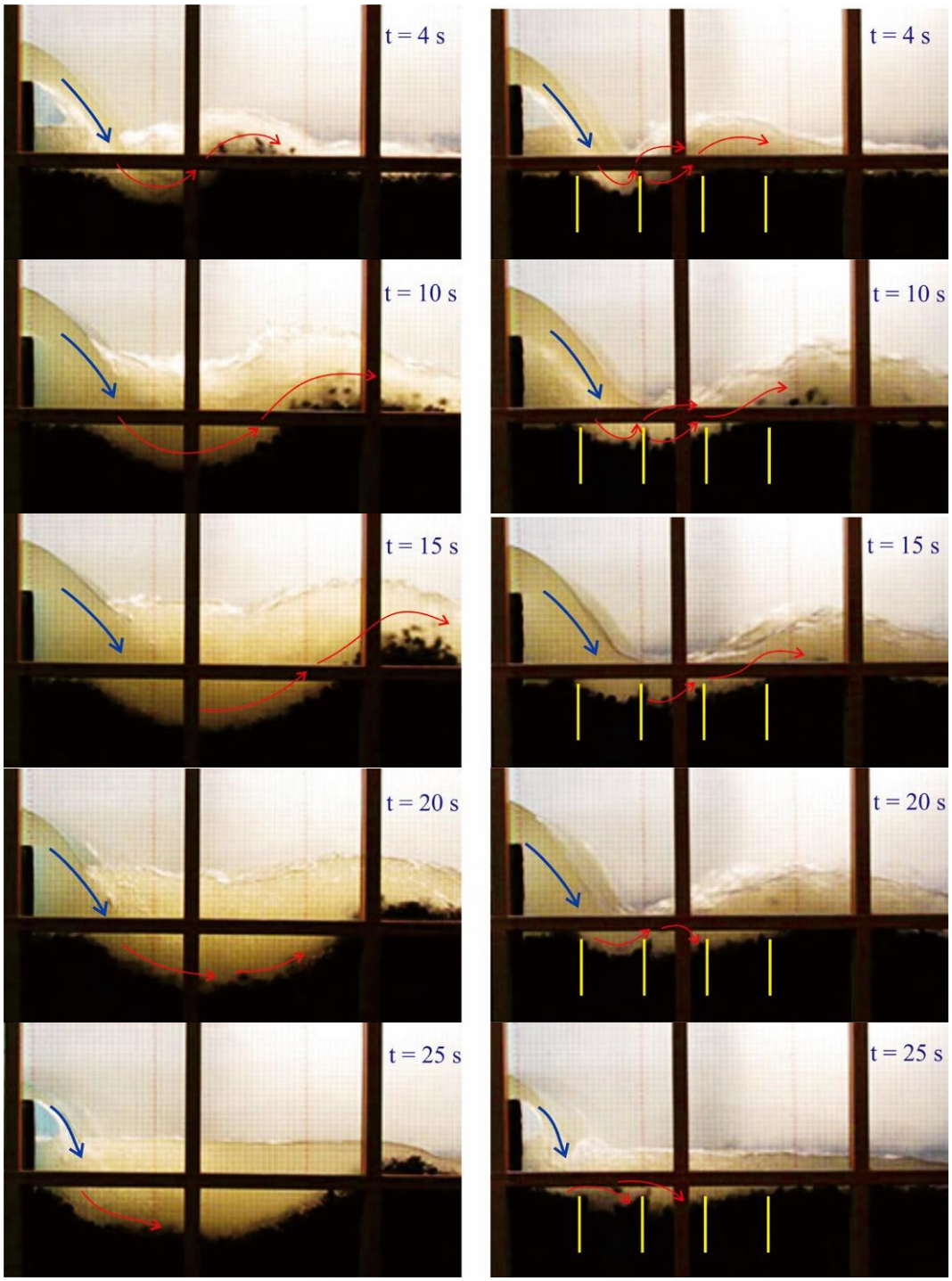

Figure 7. Scouring process of loose material without screen (left) and with a set of the screens for $L_c/(\Delta D_m) = 5.33$ (right). Blue arrows are the overflow jet, the red arrows are the directions of material transport.

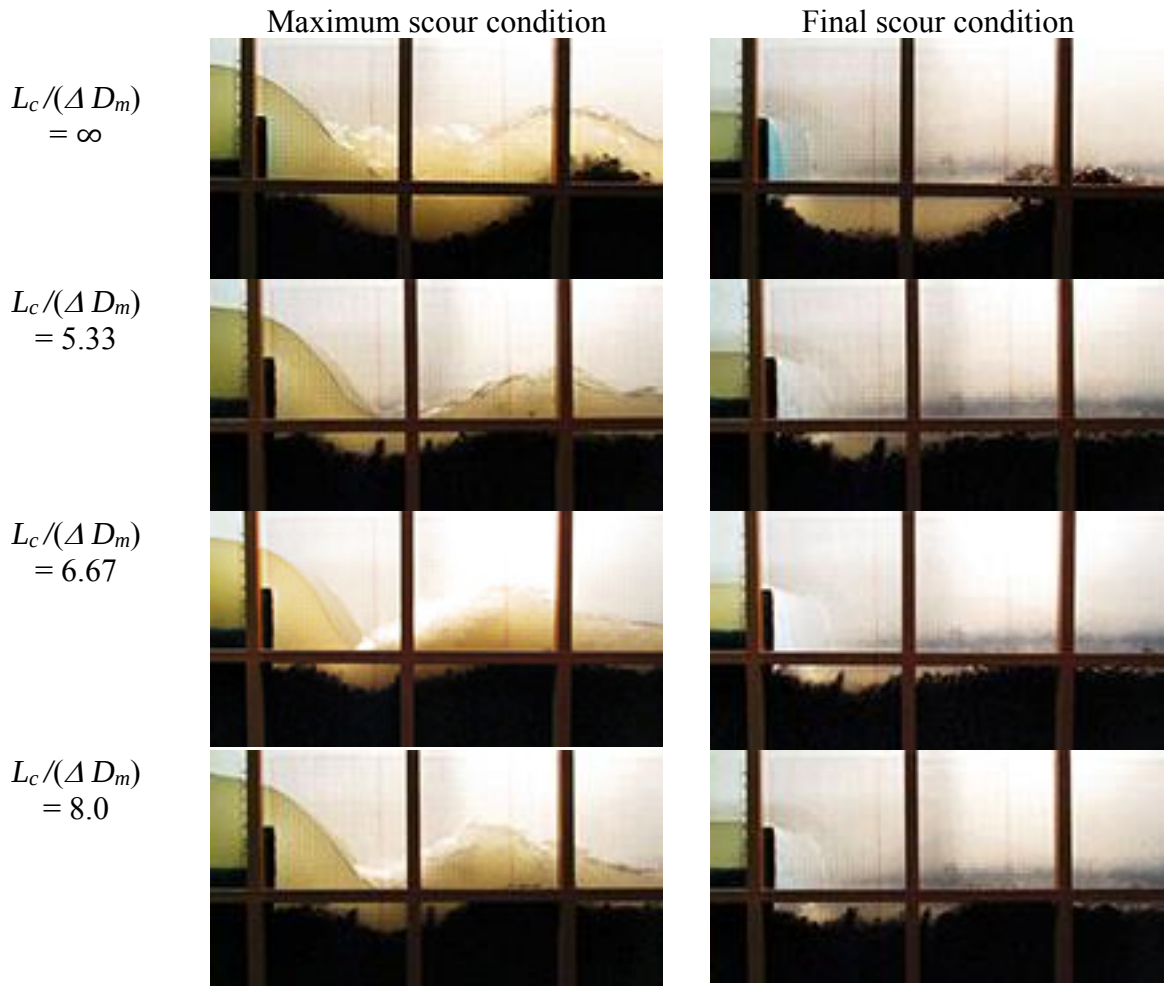

Figure 8. Maximum scour (left) and final scour(right) in various distances of the screens

The installation of the vertical screens within the bed material has been reported by (Warniyati et al. 2019) to significantly reduce the scour depths. In this research, it was found that the horizontal distance between the screen plays an important role to limit the vertical movement of the gravel and hence the scour depth. Referring to Equation (2), the effect of the screen on the scour depth and scour length are provided in Figure 9 and Figure 10. Figure 9 and 10 show that both the maximum scour depth and the scour length are gradually increased depending on the duration of the tsunami overflow.

Figure 9 reveals that the installation of the screen within the loose bed material significantly reduced the scour depth. The jet easily dragged the gravel and flushed them downstream to create longer scour holes. In Case 1 ($L_c/(\Delta D_m) = \infty$), the scour depth reached a half of the seawall height. In Case 2 ($L_c/(\Delta D_m) = 5.33$, 6.67, and 8.0), the screen blocked the transport of bed material and reduced the scour depth. The average reduction of scour depth were about 50%, 43%, and 34% for $L_c/(\Delta D_m) = 5.33$, 6.67, and 8.0 respectively. Figure 10 reveals that the total scour lengths are almost the same despite of the distances between the screens. The scour length reduction was about 25% from that of Case 1.

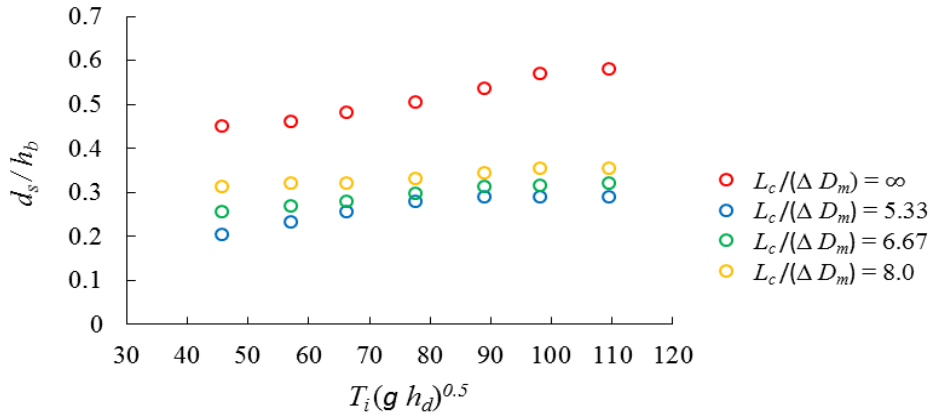

Figure 9. Nondimensional scour depth

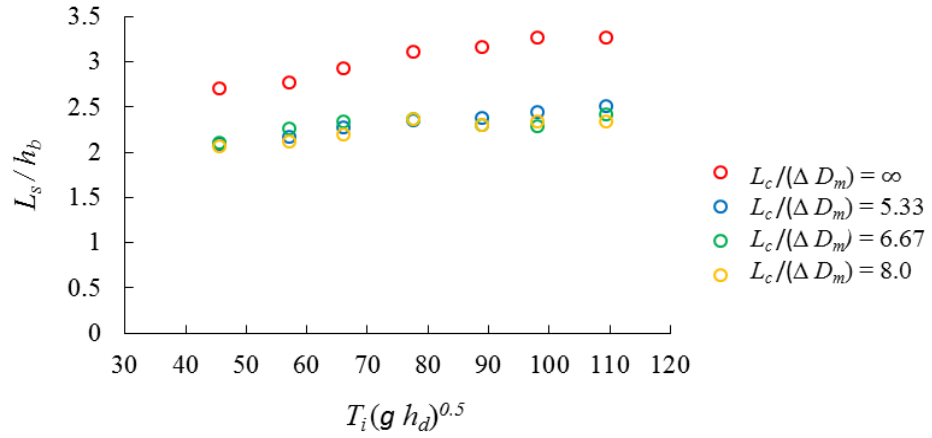

Figure 10. Nondimensional scour length

5 CONCLUSIONS

The research concluded the following:

1. The scouring process depends on the tsunami hydrograph that overflows the seawall.
2. Both the maximum scour depth and the scour length increase with the increasing tsunami overflow duration.
3. The installation of vertical screens within the loose boulder bed (modeled using gravel) effectively reduced both the scour depth and the scour length.
4. The reductions of the maximum scour depths due to the vertical screens were approximately 50%, 43%, and 34% for $L_c/(\Delta\ D_m)$ = 5.33, 6.67, and 8.0, respectively, while the scour lengths were reduced by 25 % for all scenarios.

ACKNOWLEDGEMENTS

This research was supported by the Indonesia Endowment Fund for Education (LPDP) Ministry of the Finance Republic of Indonesia who provided the doctoral scholarship for the first author. Supporting funds for this research was also provided by Universitas Gadjah Mada through a Thesis Recognition Program. Our gratitude also goes to the Hydraulics Laboratory Department of Civil and Environmental Engineering Universitas Gadjah Mada that has supported the experiment. The help of Mr. Kasiman for setting up the model is highly appreciated.

REFERENCCES

Adduce, C., and Michele, L. R. 2006. "Local Scouring due to Turbulent Water Jets Downstream of a Trapezoidal Drop: Laboratory Experiments and Stability Analysis." *Water Resources Research* 42(2):1–12

Bormann, N. E. and Pierre, Y. J. 1991. "Scour Downstream of Grade-Control Structures." *Journal of* Hydraulic *Engineering* 117(5):579–94

Dargahi, B. 2003. "Scour Development Downstream of a Spillway." *Journal of Hydraulic Research* 41(4):417–26.

Dey, S., and Rajkumar, V. R. 2007. "Scour below a High Vertical Drop." *Journal of Hydraulic Engineering* 133(5):564–68.

Fritz, H. M., Phillips, D. A., Okayasu, A., Shimozono, T., Liu, H., Mohammed, F., Skanavis, V., Synolakis, C.E., Takahashi, T. 2012. "The 2011 Japan Tsunami Current Velocity Measurements from Survivor Videos at Kesennuma Bay Using LiDAR." *Geophysical Research Letters* 39(2):1–6.

Gioia, G. and Bombardelli, F. A. 2005. "Localized Turbulent Flows on Scouring Granular Beds." *The American Physical Society* 14501(July):1–4.

Guan, D., Liu, J., Chiew, Y., and Zhou, Y. 2019. "Scour Evolution Downstream of Submerged Weir in Clear Water Scour Conditions." *Water* 11(17):1–10.

Ishikawa, N., Beppu, M., Mikami, T., Tatesawa, H., and Asai, M. 2011. "Collapse Mechanism of Seawalls by Impulsive Load due to The March 11 Tsunami." *9th International Conference on Shock & Impact Loads on Structures* 1–12.

Jayaratne, M. P. R., Premaratne, B, Adewale, A., Mikami, T., Matsuba, S., Shibayama, T., 2016. "Failure Mechanisms and Local Scour at Coastal Structures Induced by Tsunami." *Coastal Engineering Journal* 58(4): 1640017.

Matsushita, H.. 2012. “Breakwater Reinforcement Method against Large Tsunami.” *Nikken Kogaku Co., Ltd., Japan* 1–20.

Mitobe, Y., Adityawan, M. B., Tanaka, H., Kawahara, T., Kurosawa, T., and Otsushi, K. 2014. “Experiments on Local Scour Behind Coastal Dikes Induce by Tsunami Overflow.” *Coastal Engineering Proceedings* (January).

Sulianto, A. A, Murakami, K., Tokutomi, Y., and Ueno, K. 2014. “Local Scouring of Gravel Mound due to Tsunami Overflow and Its Countermeasure.” *Journal of Japan Society of Civil Engineers* 70(2):606–11.

Triatmadja, R. 2010. *TSUNAMI Kejadian, Penjalaran, Daya Rusak Dan Mitigasinya*. Yogyakarta: Gadjah Mada University Press.

Triatmadja, R., Hijah, S.T., Nurhasanah, S., 2011, Scouring Around Coastal Structures Due to Tsunami Surge, *6th Annual International Workshop & Expo on Sumatra Tsunami Disaster & Recovery 2011, In Conjunction with 4th South China Sea Tsunami Workshop*

Tsujimoto, G., Mineura, R., Yamada, F., Kakinoki, T., and Uno, K. 2014. “Scouring Mechanism behind Seawall from Tsunami Overflow and Optimum Conditions to Reduce Tsunami Energy with an Artificial Trench.” *Coastal Engineering Proceedings* 1(34):38.

Wang, D., Li, S., Arikawa, T., and Gen, H. 2016. “ISPH Simulation of Scour Behind Seawall Due to Continuous Tsunami Overflow.” *Coastal Engineering Journal* 58(3):104–15.

Warniyati, Triatmadja, R., Yuwono, N. and Bangguna, D.S. V. L. 2019. “Design of a Facility for Tsunami Run up Generation to Study Tsunami and Seawall Interaction.” *Journal Of The Civil Engineering Forum* 5(1):9–16.

Warniyati, Triatmadja, R., Yuwono, N., Legono, D., and Supraba, I. 2019. “Simulation of Scouring due to Tsunami at Downstream of a Seawall.” *Proceedings of the 38th IAHR World Congress* 5658–67.

Yeh, H., Sato, S., and Tajima, Y. 2013. “The 11 March 2011 East Japan Earthquake and Tsunami: Tsunami Effects on Coastal Infrastructure and Buildings.” *Pure and Applied Geophysics* 170(6–8):1019–31.

Yoshizuka, N., Matsushita, H., Nakanishi, T., Nishimura, H., and Oguma, K. 2018. “Disaster Prevention Facilities and Marine Environment Improvement Effect.” *Proceedings of the 34th PIANC-World Congress*.

ISSN 8755-6839

SCIENCE OF **TSUNAMI HAZARDS**

Journal of Tsunami Society International

Volume 39 **Number 3** **2020**

RADAR SUBSYSTEMS OF AUTONOMOUS MOBILE ROBOTIC SYSTEMS FOR STUDYING TSUNAMI IN THE COASTAL ZONE

P. Beresnev, A. Kurkin, A. Kuzin, A. Myakinkov, E. Pelinovsky, A. Ryndyk, S. Shabalin

Nizhny Novgorod State Technical University n.a. R.E. Alekseev, Nizhny Novgorod, RUSSIA.

ABSTRACT

The problems of using robotic systems for survey and registration of tsunami tracks in hard-to-reach places are discussed. The description of such a complex with good operational characteristics, developed at the Nizhny Novgorod State Technical University n.a. R.E. Alekseev is given. A solution is presented that allows to equip an autonomous mobile robotic complex with a sensor of the own production and increase its cross-country ability. A method for constructing an antenna array, which allows achieving optimal characteristics in terms of maximum detection range and angular resolution is proposed. This result is achieved due to the fact that the entire geometric aperture of the antenna is "filled" with elements (columns) with an array pitch of half the wavelength. In this case, the placement of the receiving sub-arrays at the edges of the substrate forms the largest aperture under the conditions of the problem been solved and allows the use of the classical method of beam-forming when working in the far zone. An example of constructing an antenna array providing the formation of beams with a width of 5° in the sector of the far-field angles is considered. Application of the proposed solution allows you to expand the detection area of objects.

***Keywords**: coastal monitoring, marine hazards, autonomous mobile robot, radar, antenna array*

1. Introduction

In this century, the tsunami problem has come to the fore, resulting in the highest number of casualties compared to other natural disasters. Fifteen years ago, the strongest earthquake in the Indian Ocean around the coast of Indonesia on December 26, 2004 with a magnitude of 9.3 led to a tsunami that turned out to be devastating for many countries in the Indian Ocean and led to the death of about 300 thousand people [1-5]. An earthquake of March 11, 2011 off the coast of Japan with a magnitude of 9.0 caused a tsunami with a maximum height of about 40 m and led to a technological disaster: the destruction of the Fukushima nuclear power plant [5-9]. On average, a global tsunami occurs almost every month, but only one in ten (about once a year) causes damage. The highest height on land that the tsunami wave reached in the post-war years is 524 m; it happened on July 9, 1958 in Alaska, when a giant landslide with a volume of about 80 million cubic meters descended from the slopes of Mount Fairweather into Lituya Bay [10]. National and international tsunami warning services have been established, and their effectiveness is increasing all the time (especially in forecasting distant tsunamis). Now the forecasting of the tsunami and its consequences has become a practical matter: plans for evacuations are communicated to residents, training of the population is arranged, protective devices are being built, etc.

The tsunami also does not bypass Russia. The most destructive in post-war history was the tsunami on November 4-5, 1952, when a wave with a height of about 10 m caused significant damage to the city of Severo-Kurilsk on the Paramushir Island, and many of its inhabitants died [10, 11]. In this century, several large tsunamis happened in the Russian Far East. Thus, a tsunami 2 m high was recorded on Sakhalin during the 2007 Nevelskoye earthquake [12, 13]. The Kuril tsunamis that occurred on November 15, 2006 and January 13, 2007, were over 10 m high and caused damage on the American coast [14-16]. Distant tsunamis that came from Samoa in 2009 and Chile in 2010 were also recorded by Russian stations [17]. Finally, the 2011 tsunami led to the breaking of the ice cover in the Kuril Islands [9].

Tsunamis occurred not only in the Russian Far East. About 20 tsunami events were registered in the Black Sea [18-20], and about 10 - in the Caspian Sea [21]. Tsunami-like phenomena also occur in inland water bodies of Russia: on rivers, lakes and reservoirs [22-24]. To understand the physics of tsunamis and to develop methods to mitigate tsunami damage, it is essential to have reliable data on the characteristics of tsunamis onshore. Survey of tsunami trails is usually carried out after all devastating tsunamis, as a rule, by national teams and using various methods. Since the 1992 tsunami in Bali (Indonesia), many tsunamis have been surveyed by international expeditions, which contributed to the development of uniform standards for conducting such expeditions and a list of characteristics that must be obtained during the survey. This experience is summarized in [25]. One of the authors of this article (Pelinovsky E.N.) began to take part in international tsunami expeditions since 1993 (Okushir tsunami in the Sea of Japan), and the experience gained is reflected in publication [26]. During the survey, an interrogation of the population is usually carried out, as well as measurements of the visible traces of the tsunami (run-up and wave heights, time of arrival, number of waves, polarity of waves). However, as a rule, the expedition manages to reach the place a week or two after the event that has already happened, when some of the tsunami witnesses

some of the visible traces of the tsunami disappear due to storms and rains, as well as during have already left the area of the disaster and restoration work. Nevertheless, the data obtained during the expedition are invaluable and are the main source for further actions to improve the methods of tsunami prediction.

Over the past 20 years, new tsunami survey techniques have begun to be developed that provide tsunami data in hard-to-reach areas or better plan tsunami expeditions. In particular, aerial photography from helicopters and drones has now begun to be used to survey tsunami traces over a vast area, see, for example, the article on the survey of the tsunami on the island of Sulawesi in 2018 [27]. Another area of study of tsunami traces in hard-to-reach places is the use of autonomous mobile robotic systems used in our team.

This present article describes an autonomous mobile robotic complex with good performance characteristics, developed at the Nizhny Novgorod State Technical University n.a. R.E. Alekseev. A solution is presented that allows to equip it with a sensor of our own production and increase its cross-country ability. A method for constructing an antenna array is proposed, which makes it possible to achieve close to optimal characteristics with respect to the maximum detection range and angular resolution.

2. Brief information about the autonomous robotic complex

One of the examples of robotic systems for monitoring the situation in the coastal zone is an autonomous mobile robotic complex (AMRK) [28-31], developed by the research team of the NNSTU n.a. R.E. Alekseev. This complex is equipped with a shipborne radar MRS-1000 (speed of a circular view of space from 12 to 24 rpm, operating frequency range from 9300 to 9500 MHz, transmitter power adjustment range of 28 dB, device protection degree IP65), a LIDAR LMS511Pro light detection system, video camera AXIS Q6045-E, differential positioning system GPS / GLONASS OS-103 (positioning error in motion mode not more than 30 cm) and weather station Vaysala WX520 (Fig. 1).

An autonomous mobile robotic complex (Fig. 1) is capable to carry out continuous monitoring of the coastal zone in any climatic conditions and on any type of support base due to the possibility of installing three different types of movers. The wheeled mover is designed for use on hard soil, as well as in dry and wet soils. The caterpillar type of mover allows you to increase the efficiency of the complex when driving in hard-to-reach places, such as sandy terrain, wet soils, snow. The rotary-screw type of mover device can be used to operate in swamps and flooded areas.

In May-June 2016 on the coast of Sakhalin Island, field tests of an experimental AMRK were carried out. The purpose of the experimental research on the coast of Sakhalin Island was to evaluate the effectiveness of the AMRK functioning and to perform typical maneuvers to study the mobility of the developed chassis. On the basis of experimental research by a team of performers, it was concluded that a number of constructive measures must be taken to increase the mobility of the complex and the effectiveness of the tasks assigned.

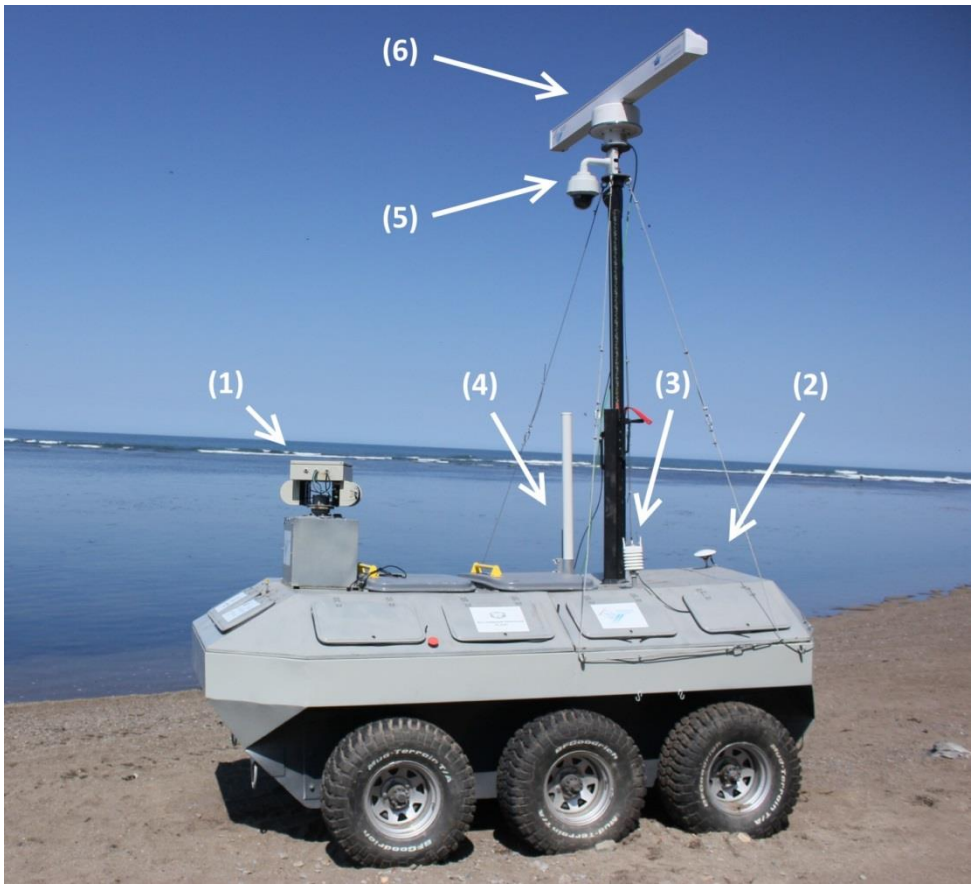

Fig. 1. Autonomous mobile robotic complex: 1 – LIDAR LMS511Pro;
2 – OS-103 positioning system antennas; 3 – Vaysala WX520 weather station;
4 – Rocket M2 omnidirectional Wi-Fi antenna; 5 – AXIS Q6045-E video camera;
6 – MRS-1000 circular view radar

The first one concerns with the development of an independent adaptive suspension. Currently, AMRK does not have a suspension, which limits the operation of the complex on hilly and mountainous areas, and also increases the risk of damage to expensive measuring equipment both as a result of the AMRK overturning and as a result of shock loads transmitted through the chassis body. Also, during the tests, it was revealed that one of the problems in creating autonomous systems is the need for automatic route correction. A deviation from the course can be the result of several reasons, including the heterogeneity of the soil, its viscosity, and massive obstacles along the way. Feedback control is required to implement the route correction system. Control with feedback is required to implement the route correction system. Such a system should include a radar system, which is currently considered as one of the key technologies for automated piloting of vehicles [32, 33].

3. Existing approaches to the construction of antenna arrays of radar systems

The most important task in the design of a radar system is the development of an antenna. The task of optimizing the architecture of the antenna system becomes especially urgent in the case of designing small-sized radars, when restriction on the geometric dimensions is one of the determining factor. Such radars include automotive radars, which are the object of analysis in this work. Antenna arrays (AR) are almost always used in the structure of modern automobile radars. It is caused by the flexibility of digital formation of the specified directivity characteristics, which is necessary to implement the required radar operating modes. The complexity of their design is determined by the contradictoriness of the requirements. In order to form a narrow beam of the directivity pattern (DP) providing the required angular resolution, corresponding antenna aperture is required. To provide unambiguous measurement of the angular coordinates within wide sector (so called near region from 90 to 120 degrees) we should exclude the arising of interference maximums of DP. In this case, we should provide the number of equivalent receive channels corresponding to the quantity of elements placed with the pitch of the half wavelength.

There are two traditional ways to solving this problem. First one is using of separated receive channels for each element of the array. For example, to ensure the beam width of the receiving antenna in azimuth of five degrees, sixteen to twenty array elements are required, depending on the weight function that determines the level of the side lobes. The requirement associated with cost reduction defines restrictions of the number of receiving channels, since not only the complexity and number of receiving and transmitting modules, but also the number of ADCs, the required throughput, and the performance of the digital processing system depend on the number of receiving channels. In practice, the number of receiving channels in the automotive radar should be either less than the number of array elements, or the array should be sparse. The construction of a sparse antenna array, when the distance between the elements (columns) significantly exceeds half wavelength, leads to energy losses compared to filled arrays. In addition, interference lobes are formed in the directivity pattern.

The second and widely used approach is use of MIMO (Multiple Input Multiple Output) technology [34]. In this case, radiation and the corresponding coherent processing of orthogonal signals help to exclude the interference maximums, but the losses associated with

the sparseness of the aperture remain. However, in some cases, automotive radar developers use this approach [35, 36] if energy requirements are not critical. This situation may occur when building medium and short range radars (up to 100 m).

4. Optimization of the structure of the radar antenna array

The most suitable for building the required antenna array from the point of view of maintaining the number of elements and reducing the number of channels is the option associated with combining columns into subarrays. In this case, the antenna aperture can be completely filled with the elements, but the distance between phase centers can be several times greater than the wavelength. This ideology is inherent in most modern long-range radars.

A schematic representation of the antenna aperture of an automotive radar is shown in Fig. 2. Suppose that there is a restriction on the total size of the antenna array, and its maximum width is determined by L_A. One part of this aperture L_{tr} can be used to place elements of a transmitting antenna, another part L_{rc} can be used for receiving array. The vertical size of the transmitting and receiving antennas $H_{tr,rc}$ can be different, for example, due to the peculiarities of the placement of integrated transceiver modules on the substrate and the tracing of the feed lines.

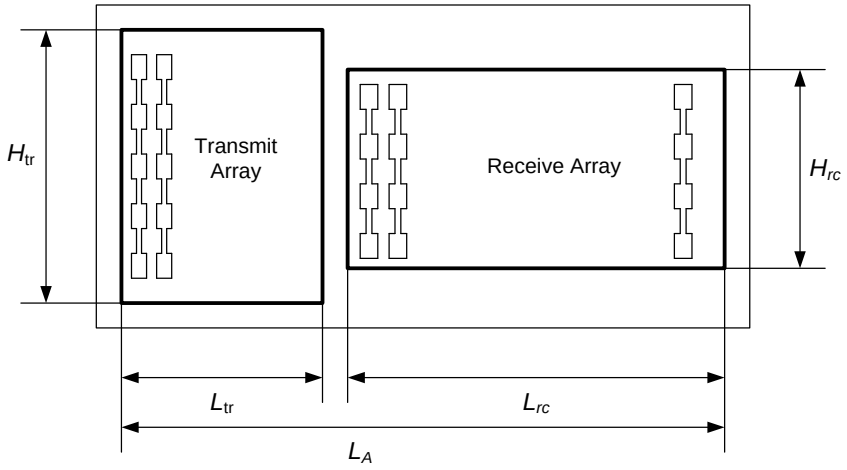

Fig. 2. Illustration for calculating the optimal ratio of the aperture sizes of the transmitter and receiver

In accordance with the basic radar equation [38], the signal power at the output of the receiving antenna of the radar is proportional to the product of the gain of the transmitting antenna G_{tr} and the effective aperture area of the receiving antenna A_{rc}:

$$P_{rc} \sim G_{tr} A_{rc}. \quad (1)$$

It is known, that the gain of a flat aperture is determined by the ratio of its effective area to the square of the wavelength ($G_{tr} = 4\pi A_{tr} / \lambda^2$), as well as the fact that the effective area of the

apertures is proportional to their geometric area (accurate to the utilization factor), which is equal to the transmitting and receiving antennas respectively $S_{tr} = H_{tr} L_{tr}$, $S_{rc} = H_{rc} L_{rc}$, we see that the output power of the receiver will be maximum when the product ($H_{tr} L_{tr}$) ($H_{rc} L_{rc}$) is maximal. According to Fig. 2, $L_{rc} \approx L_A - L_{tr}$. Then, in order to maximize the power entering the receiver, with the given restrictions on the height of the apertures, it is necessary that the condition for maximizing the product $L_{tr} (L_A - L_{tr}) = L_{tr} L_A - L_{tr}^2$ is fulfilled. To determine the maximization condition, we equate to zero the derivative of this expression with respect to L_{tr}. As a result, we obtain a simple ratio:

$$L_{tr|Ptr = max} = L_A/2. \quad (2)$$

Thus, regardless of other factors, the maximum range of the radar with the antenna configuration under consideration, while maintaining its total geometric area, will occur when the total antenna aperture is divided equally between the transmitting and receiving antennas. Figure 3 shows the results of calculating the signal-to-noise ratio at the input of an automotive radar receiver when a signal is reflected from a target with an effective scattering area of 0.2 m^2 at a distance of 100 m when using the 77 GHz FMCW radar. The frequency deviation is assumed to be equal to 200 MHz, the radiated power is 20 mW, the noise coefficient of the receiver is 13 dB, the total aperture size is L_A = 14 cm.

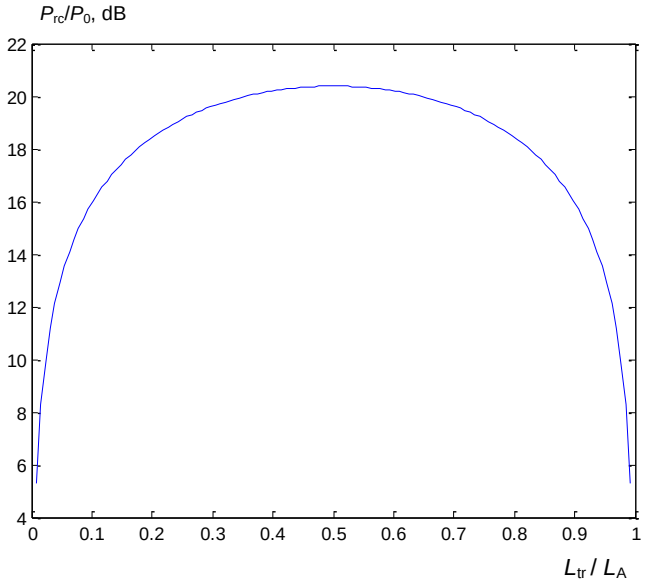

Fig. 3. Dependence of the signal-to-noise ratio at the receiver input on the relative size of the transmitting antenna

It can be seen from the graph in Fig. 3 that the value of the signal-to-noise ratio at the receiver input, which has a maximum at $L_{tr} = L_A/2$, decreases slowly when the area ratio changes, up to the values when the aperture of one of the antennas is not more than 0.2 of the total aperture.

It should also be noted that with a parallel method of irradiating the viewing sector, the beam width of the transmitting array should not be less than the width of this sector itself. A typical value of the width of the radar sector of view in the far zone is 12 ... 15 degrees. At the same time, while the columns of the transmitting antenna are spaced with a pitch equal to half of the wavelength, there is no sense to use more than eight…ten columns for transmission in the far zone. Thus, if the requirements in respect to the whole aperture allow the total number of columns to be more than 16, it is worthwhile to use additional array columns to receive the signal.

The angular resolution is determined by the width of the main lobe of the spatial ambiguity function [39], which coincides with the antenna directivity pattern as function of the angular coordinate α if antenna is matched with the direction to the source of reflection. The directivity pattern of a transceiver antenna is calculated as a Fourier transform of the amplitude-phase distribution of the field along its aperture:

$$\Phi(\alpha) = \int_{-L_A/2}^{L_A/2} U_A(x) e^{j2\pi x \sin\alpha/\lambda} dx\,, \tag{3}$$

where L_A – antenna aperture size.

In the case under consideration, the amplitude-phase distribution $U_A(x)$ should be understood as the convolution of the field distributions over the aperture of the transmitting array $U_{tr}(x)$ and the receiving array $U_{rc}(x)$:

$$U_A(x) = \mathrm{conv}\{U_{tr}(x), U_{rc}(x)\}. \tag{4}$$

The beam width Δα of the antenna DP Φ(α) determined by (3) is defined by the ratio of the wavelength to the antenna aperture:

$$\Delta\alpha = k\lambda/(L_A \cos\alpha), \tag{5}$$

where coefficient k depends upon the character of function $U_A(x)$.

For the case of uniform amplitude distribution $k \approx 0.8$. This is easily illustrated by the example of linear antenna aperture. When its length is equal to one wavelength, the beam width is approximately equal to π/4 by the half power level and strongly to π/2 by between zeros. This coefficient falls when the distribution $U_A(x)$ has maximal values at the bounds of the aperture and rises when in the middle. The same time, distribution providing minimizing the beam width, follows to the rising of side lobes of DP.

In the case when the apertures of the transmitting and receiving antennas are the same, the function $U_A(x)$ has a accented maximum and monotonically decreases relative to this maximum. For example, with a uniform field distribution $U_A(x)$ has the form of a triangle. Such a form of this function is disadvantageous from the point of view of minimizing of

coefficient k in (5). To decrease k, it is desirable that the function $U_A(x)$ grows to the edges of the aperture, or at least remain uniform. While maintaining the "integrity" of the transmitting and receiving apertures, this is possible if the size of one of them is minimal, and the other, on the contrary, occupies a large part of the antenna aperture. This situation corresponds to the case when, for example, the transmitter is built on the basis of small number (for example, one or two) columns of the antenna array, and the receiving part of the antenna contains the maximal number of columns. Figure 4 shows the dependence of the beam width of the resulting directivity pattern of the transmitting and receiving arrays depending on the ratio of the size of the transmitting aperture to the total size of the antenna. This graph is built for the radar with the same parameters as the graph in Fig. 4.

Figure 4 demonstrates that the beam width with the maximum use of the antenna aperture for the receiving channels is less than the maximum beam width with an equal distribution of the aperture between the transmitter and receiver channels by about 1.4 times.

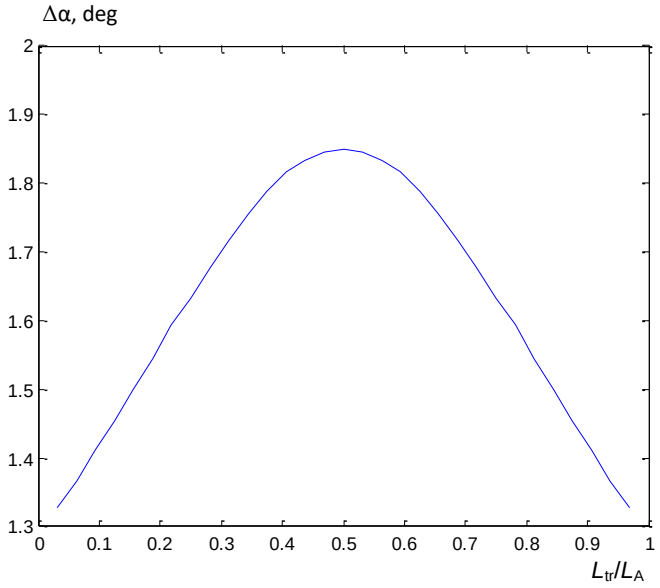

Fig. 4. Dependence of the beam width of the resulting beam on the ratio of the width of the aperture of the transmitter and the entire aperture

Thus, we see that the conditions under which the maximum range of the radar and the best resolution are achieved are contradictory.

To simultaneously satisfy the requirements of maximizing the range of the radar and high angular resolution, it is necessary, on the one hand, to maintain the quasi-equal distribution of the transmit and receive apertures, on the other hand, to place the extreme elements of one of them at a maximum distance from each other. Such a "compromise" solution could be realized placing either transmitting or receiving elements at the edges of the aperture. Holding the area of the aperture actually means holding the number of elements of the array along the horizontal (azimuthal) coordinate, that is, the number of columns. It is important to remember

that, despite the narrowing of the beam, such arrangement of the elements does not increase the gain (directivity) of the antenna, since part of the energy is radiated (received) in the direction of interference beams. The appearance of interference lobes, being a fee for narrowing the main beam of the directivity pattern, leads to the need to analyze the optimal method for placing array columns and choosing the optimal weight coefficients.

There are various ways to suppress side lobes and increase gain which are considered in many articles [40-42]. The basis for the suppression (partial suppression) of the arising interference lobes of the transmitter (receiver) DP is multiplication by a narrow directivity pattern, on the contrary, of the receiver (transmitter). Good suppression of interference lobes is possible using MIMO [43].

4.1. *Topology with sparse transmitters*

One of the possible methods of constructing a transmission array, providing the aperture size increasing, is placing of transmission subarrays at the maximum distance from each other. Consider the structure of the microstrip antenna array shown in Fig. 5 (1, 2-transmitting elements, 3-receiving elements).

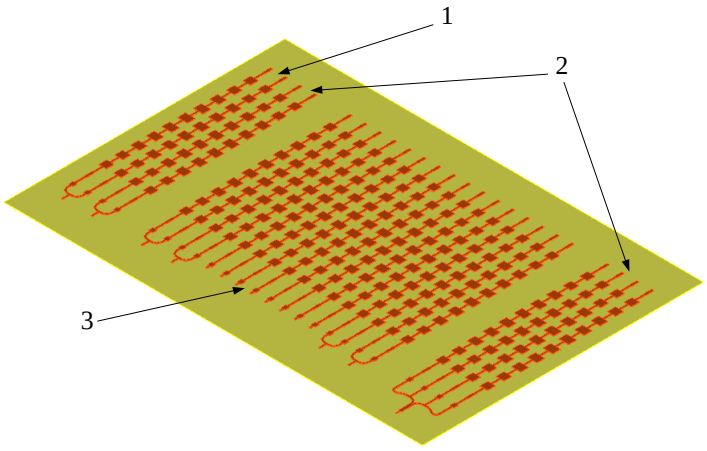

Fig. 5. Antenna array structure

The transmitting columns are located on the edges of the substrate, thereby forming the maximum possible aperture of the transmit antenna, while the receiving columns fill the space between the transmitters. In this structure transmitting elements 1 and 2 are used to irradiate the far zone. In the near zone only one transmitting subarray 1 is used to provide wide radar sector of view. Also, to eliminate influence of the interference maximums in the near zone, only eight “uncombined” elements of the receiving antenna array 3 are used. The phase of one of the transmitting channels takes the values of 0 degrees and 180 degrees, while the phase of the other transmitting channel is always equal to 0 degrees. With the antiphase switching on, the number of beams is the same, but a set of beams is orthogonal to the first one. This is illustrated by Fig. 6.

The implementation of this approach provides covering the observation sector in two sequential tacts of the transmitting arrays 1 and 2 for far zone and in one tact of transmitting array 1 for near zone. The distance between the phase centers of the transmitting subarrays is much greater than the wavelength. This circumstance determines the presence of a large number of interference lobes. The quantity and position of these lobes are determined by the distance between the transmitting elements. With the previously described geometric parameters of the phased antenna array, the repetition period of the interference lobes is approximately 11°, while the beam width is about 5°.

The most appropriate technique of constructing a receiving array taking into account both the requirements in respect to the maximizing its aperture and minimizing the number of receiving channels is use of subarrays formed of two or more columns. Figure 7 shows the receiving (curve 1), transmitting (curve 2) and resulting (curve 3) directivity patterns of the antenna during beam formation in various directions for far and near zones.

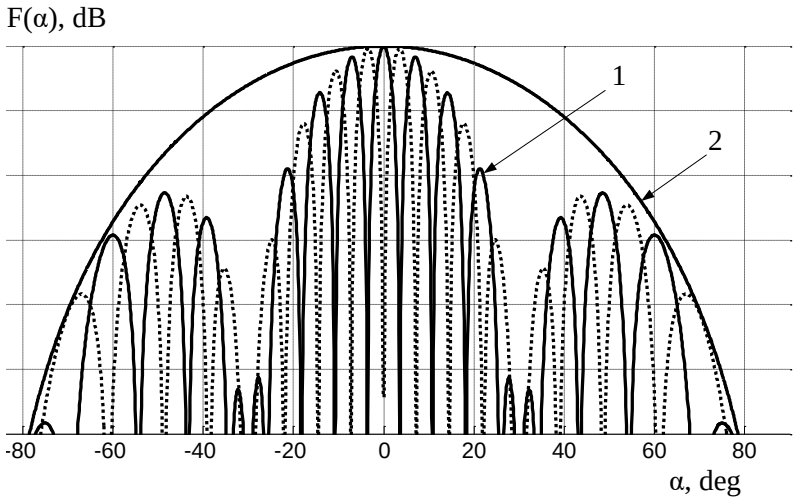

Fig. 6. Two orthogonal sets of beams of a transmission array consisting of two subarrays spaced apart at the edges of the aperture for far zone (1) and directivity pattern of the transmitting array for near zone (2)

As can be seen from Fig. 7, the resulting DP has the single main maximum that provides an unambiguous measurement of the angular coordinates. The reduction of the side lobes presents the special task which is solved by the optimization of digital beam forming.

The main disadvantage of the considered approach is the absence of the flexibility in respect to the forming of resulting beams of transceiver array. We can form receive and, therefore, resulting beams only in fixed directions of transmit beams. The same time, scanning of the observation sector with the pair of spread transmitters leads to the energy losses in comparison to the parallel irradiation of the same sector. This is caused by that loss-free scanning is possible only for the case when the gain of the scanning beam is *N*-times bigger than the gain of wide-radiating beam irradiating the whole sector. The number *N* is equal to the ratio of the

duration of the signal integration interval for the case of parallel observation to the duration when scanning, in acceptance that the whole sector observation time is the same. The same time, the gain of the pair of spread transmitters is only equal to the gain of "filled" transmitter consisting of the same quantity of elements and irradiating the whole sector.

4.2. *Topology with sparse receivers*

Achieving a high angular resolution with unambiguous azimuth measurement is also possible using the phased antenna array with maximally spaced fragments of the receiving array. This is achieved by the placing elements of receiving array, united into subarrays, at the edges of the general aperture simultaneously with placing of other elements in the central part. The middle part of the central fragment should have separated channels for each element, while side elements could be united into subarrays.

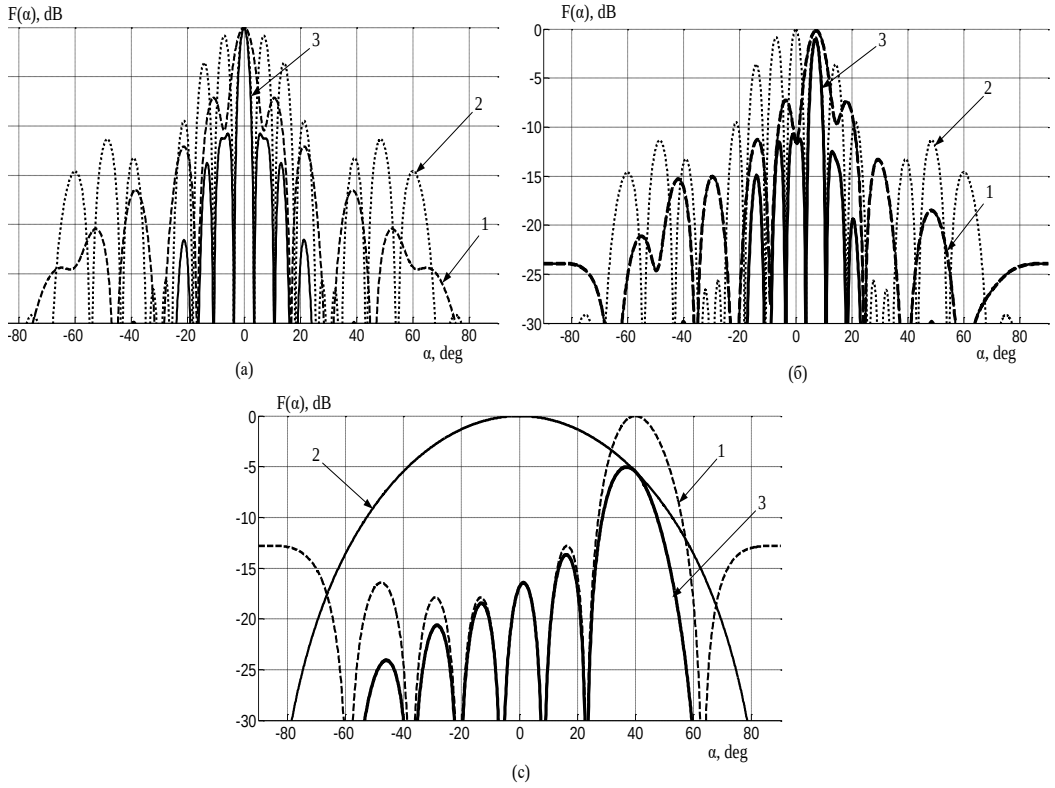

Fig. 7. Antenna directivity pattern using receiving subarrays during beam formation in the direction of (a) – 0°, (b) – 9.5°, (c) – 40° for near zone

In this case, the formation of a narrow beam of the directivity pattern of the receiving array in the azimuth plane is obtained, but interference maximums arise. Non equidistant arrangement of the array elements is known to reduce the interference maximums of the directivity pattern of a sparse antenna array [44]. With the appropriate choice of antenna array architecture, the level of the interference peaks decreases. In our case, we can easily provide different distances

between central part of the receive array and its spaced subarrays. When working in a narrow sector of view in far zone, interference maximums appear in the region of the side lobes of the transmitter's directivity pattern, and in the resulting directivity pattern these maximums are suppressed. To receive signals reflected from objects in the near zone, it is necessary to use a filled antenna array that does not have interference in the entire field of view.

The transmit part of the phased antenna array is placed between the fragments of the receiving array, exactly between its central part and edge parts. To concentrate the energy within the sector of far zone, corresponding transmit array should be wide enough, including from eight to ten columns. At the same time, in the near zone it is possible to use an antenna, consisting of only two elements included with phase shift of 180º, to form a wide viewing sector. The different width of these two transmit arrays defines the non-equidistant placement of the edge receive subarrays. Figure 8 shows the topology with receiving subarrays located at the edges of the aperture.

In the structure presented in Fig. 8, two transmitting and three receiving antennas are used. The transmitting antenna Tx_1 has a beam width of about 15º and irradiates the entire sector of the far zone. The transmitting antenna Tx_2 irradiates the near-sector with a width of at least ± 45°. To receive signals reflected from objects in the near zone, an antenna (antenna array) Rx_1 is used. The elements of this array are located equidistantly in the azimuth plane with a pitch of half wavelength.

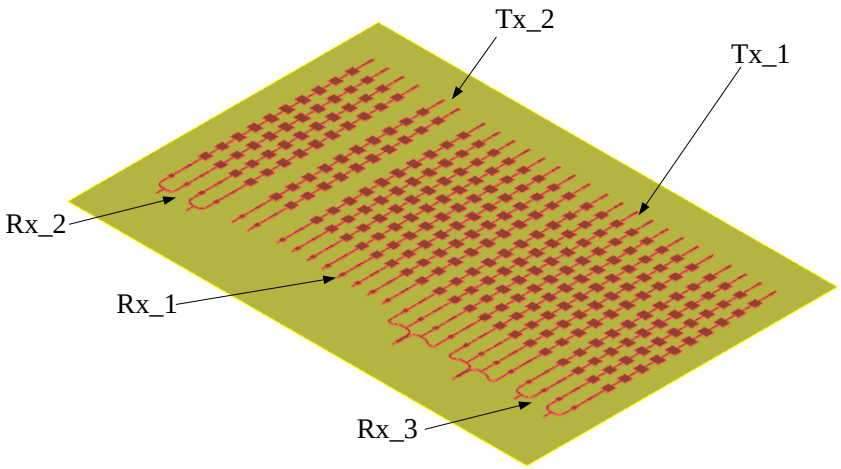

Fig. 8. Structure of the antenna array of the automotive radar

Figure 9 shows the results of electromagnetic modeling of the transmitting array, namely the directivity pattern of the transmitter Tx_1 and the level of matching of its transmitting columns with microstrip transmission lines at the center frequency of the operating range.

The beam width of the transmitter directivity pattern at half power level is 14º in E-plane and 9º in H-plane. The side lobe is -13 dB in E-plane and -15 dB in H-plane. The gain level is about 20 dB.

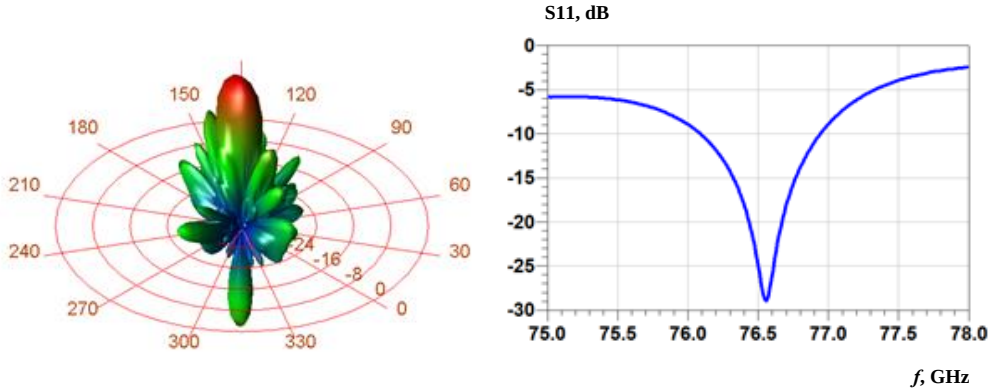

(a) (b)

Fig. 9. The directivity pattern of the transmitter Tx_1 (a) and S11-parameter corresponding to its columns (b)

The far zone antenna can be implemented as a near-field antenna, expanded with additional elements. In this case, the receiving array Rx_1 is used as the central part of the aperture of the receiving antenna for processing the far zone. In addition, two edge antennas Rx_2 and Rx_3 are used. Due to this arrangement of the antenna system, the maximum aperture of the receiving antenna for a given general geometric size is achieved, which ensures the best azimuth resolution. Fig. 10 shows the directivity patterns when placing two subarrays consisting of two columns each one as the edge antenna patterns. Curves 1 and 2 show the transmitting and receiving directivity patterns respectively, curves 3 and 4 show two beams of the resulting directivity pattern, shifted by two degrees relative to each other.

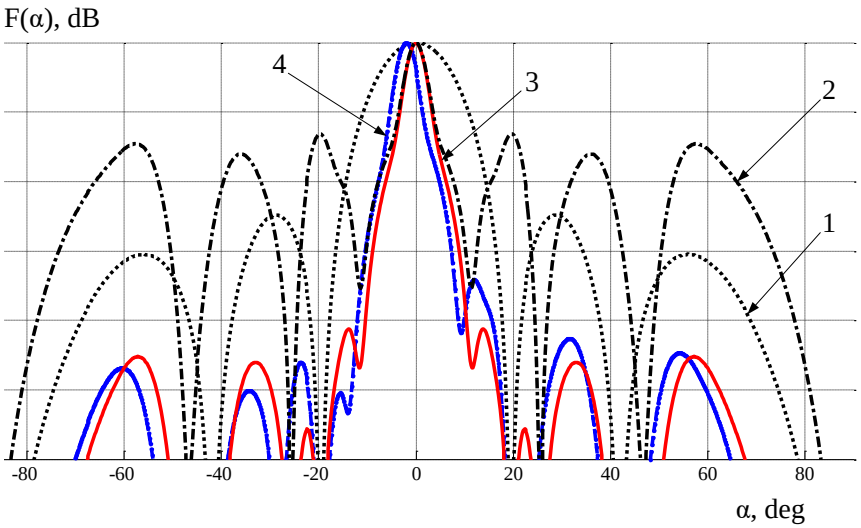

Fig. 10. The transmitting, receiving and resulting antenna directivity patterns with a distributed receiver array structure

The beam width of the resulting directivity pattern in the far zone at half power level is 5°, which is about 1.4 times less than the beam widths with the classic arrangement of the same number of array elements without spacing of receive array fragments. The side lobe level is -20 dB for the center beam and -15 dB for the side beams.

Conclusion

This article discusses the problems of using robotic systems to survey and register tsunami traces in hard-to-reach places. A description of such a complex with good performance characteristics is given. A solution that allows to equip an autonomous mobile robotic complex with a sensor of its own production and increase its cross-country ability is presented. A method for constructing an antenna array is proposed, which makes it possible to achieve close to optimal characteristics with respect to the maximum detection range and angular resolution. It is shown that in comparison with a MIMO antenna consisting of non-overlapping transmitting and receiving apertures, one of which is a sparse array, the proposed configuration provides twice as much power at the receiver output. This result is achieved due to the fact that the entire geometric aperture of the antenna is "filled" with elements (columns) with a step of half of wavelength. Physically, this means that in the case of a sparse aperture, there is a potential possibility to increase the aperture of the receiving antenna and, therefore, the received power. In this case, the placement of the receiving subarrays at the edges of the substrate forms the largest aperture under the conditions of the problem been solved and allows the use of the classical method of beamforming when working in the far zone. An example of constructing an antenna array providing the formation of beams with a width of 5° in the sector of the far-field angles is considered. Application of the proposed solution will expand the detection area of objects. In the future, it is in plan to conduct full-scale tests of automated complexes with an object detection system based on a radar of its own design in the coastal zone of Sakhalin Island.

Acknowledgments

This study has been done in Nizhny Novgorod State Technical University n.a. R.E. Alekseev (NNSTU), and supported by the Agreement № 075-11-2019-053 dated 20.11.2019 (Ministry of Science and Higher Education of the Russian Federation, in accordance with the Decree of the Government of the Russian Federation of April 9, 2010 No. 218), project «Creation of a domestic high-tech production of vehicle security systems based on a control mechanism and intelligent sensors, including millimeter radars in the 76-77 GHz range».

References

1. Titov V., Rabinovich A., Mofjeld H., Thomson R, Gonzalez F. The global reach of the 26 December, 2004 Sumatra tsunami. *Science*. 2005. V. 309. P. 2045-2048.

2. Zaitsev A.I., Kurkin A.A., Levin B.V., Pelinovsky E.N., Yalciner A., Troitskaya Yu., Ermakov S.A. Numerical simulation of catastrophic tsunami propagation in the Indian Ocean (December 26, 2004). *Doklady Earth Sciences*. 2005. V. 402. No. 4. P. 614-618.

3. Choi B.H., Hong S.J., Pelinovsky E. Distribution of runup heights of the December 26, 2004 tsunami in the Indian Ocean. *Geophysical Research Letters*. 2006. V. 33. No. 13. P. L13601.

4. Kim D.C., Kim K.O., Choi B.H., Kim K.H., Pelinovsky E. Three-dimensional runup simulation of the 2004 Indian Ocean tsunami at the Lhok Nga Twin Peaks. *Journal of Coastal Research – SI.* 2013. V. 65. P. 272-277.

5. Gusiakov V.K. Strongest tsunamis in the World Ocean and the problem of marine coastal security. *Izvestiya - Atmospheric and Ocean Physics*. 2014. V. 50. No. 5. P. 435-444.

6. Kim D.C., Kim K.O., Pelinovsky E., Didenkulova I., Choi B.H. Three-dimensional tsunami runup simulation at the Koborinai port, Sanriku coast, Japan. *Journal of Coastal Research – SI*. 2013. V. 65. P. 266-271.

7. Mori N, Takahashi T. The 2011 Tohoku Earthquake Tsunami Joint Survey Group. Nationalwide post event survey and analysis of the 2011 Tohoku Earthquake Tsunami. *Coastal Engineering Journal.* 2012. V. 54. P. 1-27.

8. Choi B.H., Min B.I., Pelinovsky E. Tsuji Y., Kim K.O. Comparable analysis of the distribution functions of runup heights of the 1896, 1933 and 2011 Japanese Tsunamis in the Sanriku Area. *Natural Hazards and Earth System Sciences*. 2012. V. 12. P. 1463-1467.

9. Kaistrenko V., Razjigaeva N., Kharlamov A., Shishkin A. Manifestation of the 2011 Great Tohoku Tsunami on the Coast of the Kuril Islands: A Tsunami with Ice. *Pure and Applied Geophysics*. 2013. V. 170. P. 1103-1114.

10. Gusiakov V.K. *Tsunami history – recorded* / A. Robinson, E. Bernard (Eds.). The Sea, V. 15. Tsunamis. – Cambridge: Harvard University Press, 2009. P. 23-53.

11. Pelinovsky E.N. *Hydrodynamics of tsunami waves*. – N. Novgorod: Institute of Applied Physics of the Russian Academy of Sciences, 1996. 276 p.

12. Zaitsev A.I., Kovalev D.P., Kurkin A.A., Levin B.W., Pelinovsky E.N., Chernov A.G., Yalciner A. The Nevelsk tsunami on August 2, 2007: Instrumental data and numerical modelling. *Doklady Earth Sciences*. 2008. V. 421. No. 1. P. 867-870.

13. Zaitsev A.I., Kovalev D.P., Kurkin A.A., Levin B.V., Pelinovskii E.N., Chernov A.G., Yalciner A. The tsunami on Sakhalin on August 2, 2007: Mareograph evidence and numerical simulation. *Russian Journal of Pacific Geology*. 2009. V. 3. No. 5. P. 437-442.

14. Levin B.W., Kaistrenko V.M., Rybin A.V., Nosov M.A., Pinegina T.K., Razzhigaeva N.G., Sasorova E.V., Ganzei K.S., Ivel'skaya T.N., Kravchunovskaya E.A., Kolesov S.V.,

Evdokimov Yu.V., Bourgeois J., MacInnes B., Fitzhugh B. Manifestations of the tsunami on November 15, 2006, on the central Kuril Islands and results of the runup heights modelling. *Doklady Earth Sciences*. 2008. V. 419. No. 1. P. 335-338.

15. Laverov N.P., Lobkovsky L.I., Levin B.W., Rabinovich A.B., Kulikov E.A., Fine I.V., Thomson R.E. The Kuril tsunamis of november 15, 2006, and january 13, 2007: Two trans-pacific events. *Doklady Earth Sciences*. 2009. V. 426. No. 1. P. 658-664.

16. Lobkovsky L.I., Rabinovich A.B., Kulikov E.A., Ivashchenko A.I., Fine, I.V., Thomson R.E., Ivelskaya T.N., Bogdanov G.S. The Kuril Earthquakes and tsunamis of November 15, 2006, and January 13, 2007: Observations, analysis, and numerical modeling. *Oceanology*. 2009. V. 49. No. 2. P. 166-181.

17. Shevchenko G., Ivelskaya T., Loskutov A., Shishkin A. The 2009 Samoan and 2010 Chilean tsunamis recorded on the Pacific coast of Russia. *Pure and Applied Geophysics*. 2013. V. 170. P. 1511-1527.

18. Dotsenko S.F. The Black Sea tsunamis. *Izvestiya - Atmospheric and Oceanic Physics*. 1995. V. 30. No. 4. P. 483-489.

19. Yalciner A., Pelinovsky E., Talipova T., Kurkin A., Kozelkov A., Zaitsev A. Tsunamis in the Black Sea: comparison of the historical, instrumental and numerical data. *Journal of Geophysical Research*. 2004. V. 109. No. C12. P. C12023.

20. Zaitsev A.I., Pelinovsky E.N. Forecasting of tsunami wave heights at the Russian coast of the Black Sea. *Oceanology*. 2011. V. 51. No. 6. P. 907-915.

21. Dotsenko S.F., Kuzin I.P., Levin B.V., Solov'eva O.N. Tsunami in the Caspian sea: Seismic sources and features of propagation. *Oceanology*. 2000. V. 40. No. 4. P. 474-482.

22. Didenkulova I.I., Pelinovsky E.N. Phenomena similar to tsunami in Russian internal basins. *Russian Journal of Earth Sciences*. 2006. V. 8. No. 6. P. ES6002-1-9.

23. Didenkulova I.I., Pelinovsky E.N. Phenomena like the tsunami in Russian internal reservoirs. *Fundamentalnaya i Prikladnaya Gidrofizika*. 2009. No. 3(5). P. 52-64.

24. Torsvik T., Paris R., Didenkulova I., Pelinovsky E., Belousov A., Belousova M. Numerical simulation of tsunami event during the 1996 volcanic eruption in Karymskoe lake, Kamchatka, Russia. *Natural Hazards and Earth System Sciences*. 2010. V. 10. P. 2359- 2369.

25. Farreras S. *Post-tsunami survey field guide* IOS. Manuals and Guides, No. 30. – Paris: UNESCO, 1998. 45 p.

26. Pelinovskij E.N. International expeditions for Tsunami. *Bulletin of Russian Foundation for Basic Research*. 1996. No 5. P. 26-30.

27. Fritz H.M., Synolakis C/E., Kalligeris N., Skanavis V., Santoso F.J., Rizal M., Prasetya G.L.Y., Liu Ph.L-F. The 2018 Sulawesi tsunami: field survey and eyewitness video analysis using lidar. *Geophysical Research Abstracts*. 2019. V. 21. P. 1-1.

28. Zaytsev A., Belyakov V., Beresnev P., Filatov V., Makarov V., Tyugin D., Kurkin A. Coastal monitoring of the Okhotsk sea using an autonomous mobile robot. *Science of Tsunami Hazards*. 2017. V. 36. No. 1. P. 1-12.

29. Kurkin A., Tyugin D., Kuzin V., Zeziulin D., Pelinovsky E., Malashenko A., Beresnev P., Belyakov V. Development of a group of mobile robots for conducting comprehensive research of dangerous wave characteristics in coastal zones. *Science of Tsunami Hazards*. 2018. V. 37. No. 3. P. 157-174.

30. Kurkin A.A., Tyugin D.Y., Kuzin V.D., Chernov A.G., Makarov V.S., Beresnev P.O., Zeziulin D.V. Autonomous mobile robotic system for environment monitoring in a coastal zone. *Procedia Computer Science*. 2017. V. 103. P. 459-465.

31. Beresnev P.O., Kurkin A.A., Tyugin D.Y., Orlov I.Y., Filatov V.I., Belyakov V.V. Experimental study of autonomous complexes motion. *Proceedings of the Fourteenth MEDCOAST Congress on Coastal and Marine Sciences, Engineering, Management and Conservation*. 2019. V. 2. P. 881-891.

32. Dickmann J., Appenrodt N., Bloecher H.-L., Brenk C., Hackbarth T., Hahn M., Klappstein J., Muntzinger M., Sailer A. Radar contribution to highly automated driving. *Proceedings of the European Radar Conference*. Rome. Italy. 2014. P. 412–415.

33. Myakinkov A.V., Sidorov S.B., Shishanov S.V., Shabalin S.A. The distributed radar system for monitoring the surrounding situation for the intelligent vehicle. *Proceedings of the 19th Int. Radar Symposium*. Bonn. Germany. 2018. P. 1-8.

34. Pirkani A.A., Pooni S., Cherniakov M. Implementation of MIMO beamforming on an OTS FMCW automotive radar. *Proceedings of the Int. Radar Symposium*. 2019. 8 p.

35. Engels F., Wintermantel M., Heidenreich P. Automotive MIMO radar angle estimation in the presence of multipath. *Proceedings of the European Radar Conference*. 2017.

36. Rohling H., Meinecke M.-M. Waveform Design Principles for Automotive Radar System. *Proceedings of the CIE Int. Conference on Radar*. 2001.

37. Shabalin S.A., Myakinkov A.V., Kuzin A.A., Ryndyk A.G. Millimeter-wave Phased Antenna Array for Automotive Radar. *Proceedings of the 20th Int. Radar Symposium*. Ulm. Germany. 2019. P. 1-8.

38. Scolnik M.I. *Radar handbook*. Third edition. The McGraw-Hill Companies. 2008.

39. Amin M.G., Belouchrani A., Zhang Y. The spatial ambiguity function and its applications. *IEEE Signal Processing Letters*. 2000. V. 7. Issue: 6.

40. Rohling H., Moller C. Radar waveform for automotive radar systems and applications. *Proceedings of the Radar Conf. 2008 RADAR'08*. Rome. Italy. 2008. P. 1–4.

41. Jasteh D., Gashinova M., Hoare E.G., Tran T.-Y., Clarke N., Cherniakov M. Low-THz Imaging Radar for Outdoor Applications. *Proceedings of the 16th Int. Radar Symposium*. 2015. V. 1. P. 203-208.

42. Vizard D.R, Gashinova M., Hoare E.G., Cherniakov M. Low-THz Automotive Radar Developments Employing 300-600 GHz Frequency Extenders. *Proceedings of the 16th Int. Radar Symposium*. 2015. V. 1. P. 209-214.

43. Zwanetski A., Kronauge M., Rohling H. Waveform Design for FMCW MIMO Radar Based on Frequency Division. *Proceedings of the 14th Int. Radar Symposium*. 2013. V. 1. P. 89-94.

44. Shabunin S.N., Chechetkin V.A., Klygach D.S., Ershov A.V., Vakhitov M.G., Dumchev V.A., Dumchev I.A. Non-equidistant antenna array with low level of side lobes. *Proceedings of the 2016 IEEE 6th Int. Conference on Communications and Electronics*. 2016. P. 230-233.

ISSN 8755-6839

SCIENCE OF **TSUNAMI HAZARDS**

Journal of Tsunami Society International

Volume 39 **Number 3** **2020**

MECHANISM OF INCREASING PREPAREDNESS TSUNAMI: OMBAK - Learning Model Development

Madlazim and Eko Haryono

e-mail:madlazim@unesa.ac.id

Physics Department, State University of Surabaya, INDONESIA

ABSTRACT

People who live in tsunami disaster-prone areas need to be prepared to mitigate potential future risks. The present study aims in developing a learning model for tsunami mitigation in Indonesia. The model used for this study adopts an ADDIE approach - an acronym for Analysis, Design, Development, Implementation, and Evaluation. The analysis section of the report evaluates the learning needs of people who live in tsunami-prone locations. The subsequent design section of the report focuses in setting the creation of a new learning model regarding the mitigation of tsunami disaster impact and destruction. The development section addresses the required needs for the development of a tsunami mitigation learning model. The implementation section aims in applying and testing the developed model. Finally, the evaluation section assesses all of the activities of the developed model. The results of the study propose a new Tsunami learning model having four phases, abbreviated as "OMBAK".

Keywords: *Mitigation, Tsunami, Learning model, OMBAK, habituation.*

Vol. 39, No. 3, page 156 (2020)

INTRODUCTION

Indonesia is a fertile country with abundant natural resources, but located in the convergence zones of very active tectonic plates characterized by high seismic and volcanic activities which can generate additional destruction by tsunamis striking the extensive coasts of the country's numerous islands. Thus, the people in Indonesia are very vulnerable to natural disasters (Paripurno et al., 2019), but the death toll could be significantly reduced with proper education of potential disasters and adequate programs of preparedness. It is very important that the people in such threatened areas receive proper education in understanding these potential disasters and in developing skills to act responsibly before and after they strike (Tranto, 2010; Brunner & Lewis, 2006), so as to avoid or minimize the risk of becoming victims (Daud, et al., 2014).

A learning model for disaster alert needs to be developed and applied for the education of elementary school students to help them with their safety and resilience before, during, and after disasters stike. Based on past disasters that have occurred in Indonesia, such learning and training are needed to save the people when disasters strike, and for the way of avoiding accidents even in their daily lives. The main problem which people in Indonesia still face is the insuffienct level of disaster awareness. Lack of awareness can increase people's risk to disaster threats (Paripurno et al., 2019). Preliminary studies at the State University of Surabaya determined that there are still many people who are lacking in all aspects of disaster preparedness, especially in knowledge, attitudes, and post-disaster evacuation skills. Such lack of understanding on how to avoid or to mitigate the impact of disasters upon their lives, is the main reason for their vulnerability. Therefore, the present study aims to develop an innovative learning model to help improve disaster preparedness, especially for that of the tsunami hazard. Such disaster preparedness programs needs to be developed, starting at the level of basic education so as to build a safety and resilience culture, especially for children and young people.

Since many natural disasters and various other hazards occur frequently in Indonesia, early training is very much needed, which should include the right way for children and younger people to save themselves when disasters strike, and also avoid accidents in their daily lives. In general, the main problem is that the Indonesian people still do not have a sufficiently high level of awareness of the potential disasters that can strike their communities. Such lack of awareness increases community risks against potential disaster threats (Paripurno et al., 2019). This fact is reinforced by the results of preliminary studies conducted at Surabaya State University which indicate that there are still many people who are lacking in the aspects of disaster preparedness, especially of disaster knowledge, disaster response attitudes, and post-disaster evacuation skills. Therefore, there is a need for research with the main objective being the development of innovative learning models that can improve community disaster preparedness and particularly for tsunamis which, in recent years, have been very destructive and have caused many deaths.

The Model

With the above mentioned main objective, the present study concentrated in a program named the *Educational Design Research* (*EDR*). According to Akker et al., (2006), educational

design research is the systematic study of designing, developing, and evaluating training interventions as solutions for complex problems in educational practice, which also aim in advancing knowledge about the characteristics of these interventions, and about the processes of designing and developing them. The research objective of such training methodology is to produce a valid, practical, and effective OMBAK Learning Model to improve community disaster preparedness. Also this type of research produces learning education tools as an operational form of the OMBAK Learning Model, namely: Semester Implementation Plan (RPS), Learning Implementation Plan (RPP), Textbooks, Student Activity Sheets (LKS), Learning Model Implementation Worksheet (LKMP), Preparedness Assessment Instrument Disasters (IPKB), and Student Response Questionnaire (ARM).

Lite

(Theo

Learning model, OMBAK

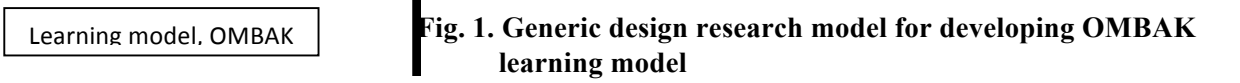

Fig. 1. Generic design research model for developing OMBAK learning model

The preparation of the OMBAK Learning Model refers to the Generic Design Research Model, according to Wademan. The steps of GDRM [8] are 1) identification of problems, 2) identification of product principles and designs tentatively, 3) theories and products temporarily, 4) making prototypes and valuing products, and 5) improving product quality. Stage of developing hypothetical learning models by modifying the generic design research model (Wademan, 2005) - presented in Fig. 1.

There are three school locations (communities) that are potentially prone to the tsunami hazard Tsunami, which are considered by the present study. First, the school community at Junior High School 2 Besuki, Bedsole village, in the Tulung Agung district. The distance from the school to Sidem beach is about 7 km. Second, the school community at Junior High School 2 Panggungrejo, Serang village, at Blitar district. The distance from the school to the beach is about 5 km. Third, the school community at Junior High School 3 Bantur, Sumberbening village, in the Malang district. The distance from the school to Balekambang beach is around 8 km. The school community referred to in this study are people within the school area consisting of a principal, two teachers, thirty-five students, one security guard, one guardian of the school, and one guardian of the canteen, so the total respondents for the three schools are 123 people.

RESULTS AND DISCUSSION

1. The OMBAK Learning Model

The tsunami mitigation-learning model that has been developed has four phases, namely Orientation, Understanding the concept of tsunami mitigation, Acting evacuation, and Correction (Evaluation). These four learning phases are called OMBAK. The following details the **OMBAK** learning model:

Table 1. Theoretical and Empirical Support from the Syntax of the OMBAK Learning Model

Theoretical Support	Empirical Support	Learning Activity	Learning Access Indicators
1. ARCS Theory (Attention, Relevance, Confidence, and Satisfaction) in order to raise curiosity and interest in learning, students must pay attention (Keller, 2010). 2. Attention (Bandura, 1977), students must pay attention to the model that will be used as a model in the learning process (Moreno, 2010). Students are intrinsically motivated through experiences that involve imagination and creativity (Eggen & Kauchak, 2013). 3. Using or changing previous knowledge and skills into creative products requires complex cognitive processes (Moreno, 2010; Eggen & Kauchak, 2013).	1. Teachers must be able to have a positive effect on student motivation in learning (Jones, Epler, Mokri, Bryant, & Paretti, 2013; Jones & Vall, 2014). 2. The results of the study indicate that motivation can have an effect on success in individuals (OECD, 2013). 3. The need for proper conditioning and preliminary preparation of student learning styles, self-efficacy, and intrinsic academic motivation in the learning process (Bembenutty, Cleary, & Kitsantas, 2013; Zimmerman & Schunk, 2008). 4. The government should always carry out disaster preparedness activities (Abidin, Bachri, Laksono, & Afandi, 2018). Disaster	**Phase 1: Orientation (O)** aims to attract student interest, focus student attention, and motivate them to play an active role in the learning process. In this phase, the virtual lab application on disaster preparedness plays an important role in the success of phases 2, 3, and 4 because the ability of lecturers to use the virtual lab application will facilitate classroom management so the students are more motivated and interactive in learning. In addition, students have been directed to understand the problems that will be solved to improve disaster preparedness.	The community is motivated in tsunami disaster preparedness

Theoretical Support	Empirical Support	Learning Activity	Learning Access Indicators
4. Advanced organizers: Directing students can help students to combine new information (Slavin, 2011). 5. Primacy effect; The Primacy effect; The tendency for items that appear at the beginning of a list is easier to remember than other items (Slavin, 2011).	preparedness activities are not specifically programmed but merely information. The areas on the banks or in the area around the river have disaster preparedness, especially mental recovery during and after disasters (Abidin, Bachri, Laksono, & Afandi, 2018).		
6. The cognitive constructivist theory by Piaget (1954, 1963), each participant is actively involved in the process of information acquisition and construction of their own knowledge (Arends, 2012). 7. Vygotsky's social constructivist theory has two implications surrounding the theory of social learning and the Zone of Proximal Development (Slavin, 2011). 8. Level of information processing, people, will handle stimuli at different levels of mental processing and will store information that has been managed through the most serious and deep processing (Slavin, 2011).	5. Authentic and meaningful problems that students find as a starting point for acquiring new knowledge (Batdi, 2014; Ibrahim, 2012; Imafuku, Kataoka, Mayahara, Suzuki, & Saiki, 2014; Stalker, Cullen, & Kloesel, 2014; Temel, 2014). 6. The government should always carry out disaster preparedness activities (Abidin, Bachri, Laksono, & Afandi, 2018). Disaster preparedness activities are not specifically programmed but merely information. The areas on the banks or in the area around the river have disaster preparedness, especially mental recovery during and after disasters (Abidin, Bachri, Laksono, & Afandi, 2018).	**Phase 2: (M)emahami (to understand)** Conceptual learning is needed to provide basic knowledge about the disaster. This basic knowledge of disaster includes knowledge of potential disaster threats, vulnerabilities, capacities, and disaster risks.	Disaster Preparedness: Communities understand tsunami disaster knowledge

Theoretical Support	Empirical Support	Learning Activity	Learning Access Indicators
9. Retention, students must do repetition so that their procedural knowledge can be remembered (Moreno, 2010).			
10. Cognitive distribution theory: Conveying ideas to others can improve their own understanding (Moreno, 2010). 11.The dual coding theory, the information presented visually and verbally, is remembered better than information that is only presented in one way (Slavin, 2011). 12.The level of information processing, people, will handle stimuli at different levels of mental processing and will store information that has been managed through the most serious and deep processing (Slavin, 2011). 13.Cognitive apprenticeship; the process when a student reaches expertise in his interaction with an expert (Slavin, 2011). 14.Positive interdependence, students need to have a positive dependence to achieve success in the process of collaborative problem	7. The results of previous studies show that students who process information seriously have better memories than those who do not (Slavin, 2011). 8. Lack of opportunities to give realistic feedback on the quality of ideas generated, this reduces student motivation and inhibits student confidence in solving problems (Munro, 2011). 9. In line with Pratiwi and Prihatiningsih (2016), with the results of the study, there is an influence of earthquake disaster management training to improve disaster preparedness. 10. Results of Havwina, Maryani, and Nandi (2016) research that experience significantly influences students' readiness with positive coefficients, which means that the higher value of disaster experience variable, the better preparedness.	**Phase 3: (B) ertind (A) k (to act)** Action is practical learning that is intended for students can have skills in the disaster, include preparedness, emergency, and recovery exercises, as well as preparing disaster management plans and contingency plans. At this stage, students are also expected to be able to apply their disaster management capabilities, both on-campus and off-campus. The outcome of the disaster learning process that is followed by these students is the profile of graduates who are knowledgeable about disaster risk reduction. After learning the practice, it is hoped that students will have a strong attitude in dealing with disasters.	Disaster Preparedness: People act correctly in the face of the tsunami disaster

Theoretical Support	Empirical Support	Learning Activity	Learning Access Indicators
solving (Moreno, 2010).			
15. *Motivation* (Bandura, 1977) students need further practice to rich more motivation (Moreno, 2010). 16. *Self-evaluation,* students must be able to evaluate the process and results of scientific creativity and collaboration as a reflection for further action (Moreno, 2010). 17. The final effect, the tendency for items that appear at the end, is easier to remember than other items (Slavin, 2011).	11. Evaluation of ideas and other thoughts can improve problem-solving abilities (Gregory, Hardiman, Yarmolinskaya, Rinne, & Limb, 2013). 12. The need for teacher evaluations of the inquiry process and problem solving of students is an important component, with no feedback gained little knowledge (Arends, 2012). 13. It can be found in public places, agencies, institutions, and so on (Utami & Nanda, 2018).	**Phase 4: (K)oreksi (to correct / to evaluate)** aims to evaluate the disaster preparedness of prospective teachers and prepare follow-up. Lecturers involve students in evaluating tsunami preparedness for the community. The instructor directs the community to prepare everything for the next meeting.	The community has Tsunami Disaster Preparedness

2. The effectiveness of the OMBAK learning model

To describe the effectiveness of the OMBAK learning model, it was tested at three schools using a qualitative approach. The qualitative approach includes: 1) Planning: plan what actions are carried out to improve, enhance, and change school communities' attitudes as a solution, 2) Application: The effort made by the researchers in term of improvement, enhancement, and desired change, 3) Observation: Observe the effect of OMBAK on students' response in the class, and 4) Reflection: Review and consider the influence of various criteria.

Data was collected using a questionnaire to measure understanding, attitude, preparedness action, and school communities' response to the learning model used. Moreover, the observation sheet was administered to collect additional data in terms of disaster readiness. Qualitative data were analyzed by following Moleong's (2007) technique, namely: 1) Analyzing all available data from various sources (interviews, observations, pictures, videos, and others); 2) Conducting data reduction by means of abstraction (making summaries and statements focus on the aims of research); 3) Selecting and grouping data based on information which has been compiled, and 4) Conducting data validation before drawing conclusions of the study. Moreover, quantitative data were analyzed by using a percentage formula (Sugiyono, 2013):

$$P_n = f/Nx\ 100\% \quad \ldots\ldots (1)$$

P_n = Success percentage of supporting factors (n=1: Understanding, n=2: Attitude, n=3: Preparadness action); f = Total score obtained by each factor; N= Maximum score for each factor.

In general, knowledge of disaster readiness is good. It was found that school communities' understanding increase from 75% to 95% in cycle II. Therefore, it was concluded that OMBAK learning model is effective in improving Indonesian disaster readiness. It is expected that this learning model could decrease the risk of disasters, such as Tsunami and earthquake, as the most happened disasters in Indonesia. See the percentage of their understanding in Fig. 2.

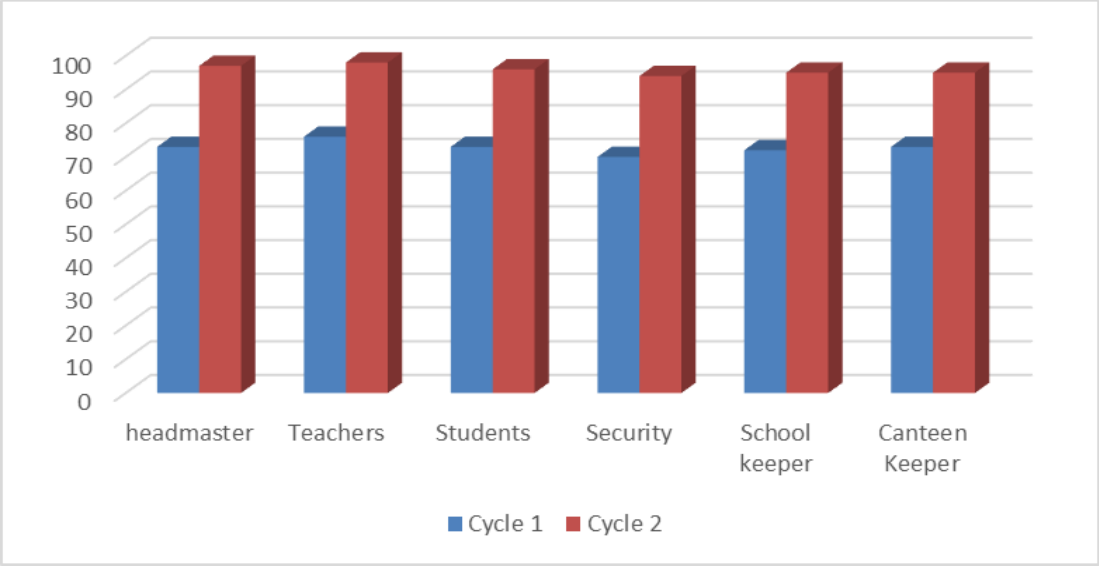

Figure 2. Comparison of subject's understanding in Cycle I and Cycle II

This result was supported by prior studies of Pribadi and Yuliawati (2009), Daud, et al. (2014), Madlazim and Supriyono 201), and Madlazim et al (2020), in which there was an increase of students' and parents' understanding after they applied the disaster preparedness educational subject. Conceptual understanding and attitude correlate with each other. With the knowledge of disaster preparedness, it will affect human attitude when a disaster occurs. In addition, attitudes based on knowledge can be utilized in the long run.

For the attitude aspect in facing the disasters, it was found that the participants' attitude varies from very appropriate to good. It was shown by their percentage increases from 74.3% (cycle I) to 96.8% (cycle II). A comparison of answers' percentages in each school can be seen in Fig. 3.

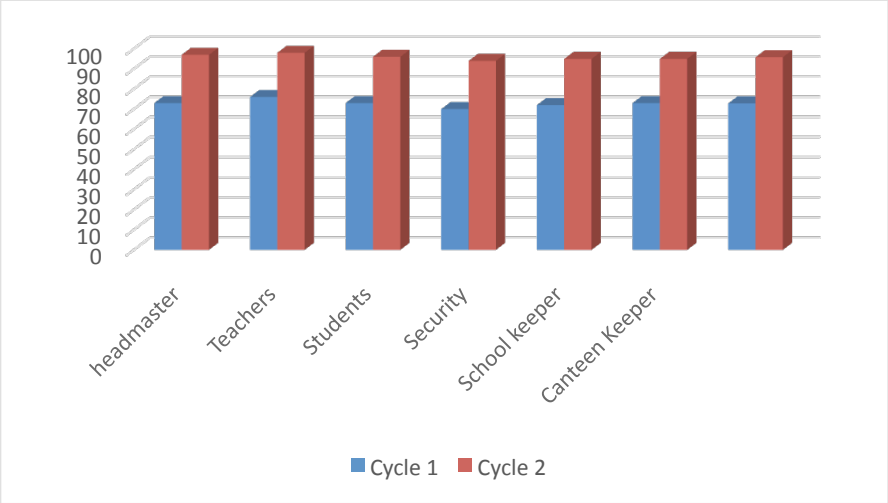

Figure 3. Comparison of school communities' attitude in cycle I and cycle II

A previous study concluded that understanding, attitude, and family support significantly affect disaster preparedness (Lenawida, 2011), and attitude is the main factor. The school communities' attitude increases by up to 23% (72.8% to 95.8% in cycle I and cycle II, respectively). The percentage comparison of each school community can be seen in Fig. 4.

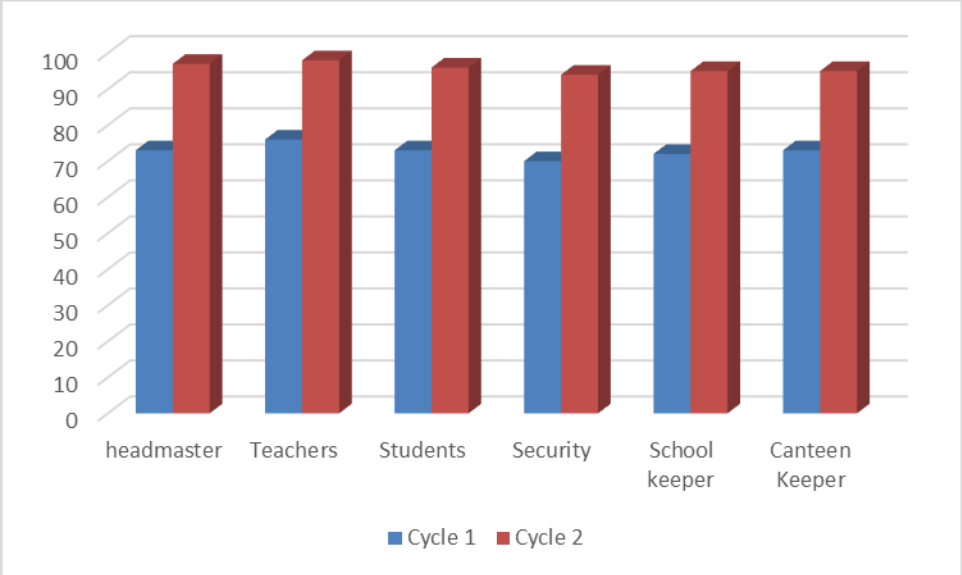

Figure 4. Comparison of school communities' attitude in cycle I and cycle II

Khairuddin et al. (2012), Madlazim and Supriyono 201), and Madlazim et al (2020) investigated the society's disaster preparedness and found that their preparedness in reducing the risk of disaster is still at the level of knowing rescue, but they do not yet have the skills for preparedness actions.

CONCLUSIONS

It has developed the OMBAK learning model, including 4 phases, that is orientation, understanding, action, and evaluation. This model is effective to significantly increase conceptual understanding, attitude, and response to mitigation.

ACKNOWLEDGEMENTS

Thanks to Dr. George Pararas-Carayannis who reviewed and corrected a partially edited draft of our paper. We wish to acknowledge with appreciation the Research and Community Service Board (DRP) of the Ministry of Research and Technology of Higher Education, who supported this research through a research contract for the Primary Higher Education Research Scheme (Surabaya State University) No. B/11637/UN38.9/LK.04.00/2020.

REFERENCES

Akker, van den, J. J. H., Gravemeijer, K. P. E., McKenney, S., & Nieveen, N. M. (Eds.) (2006). *Educational design research*. London: Routledge Taylor & Francis Group.

Abidin, Z., Bachri, A., Laksono, A.B., & Afandi. (2018). Mitigasi Bencana Dan Sosialisasi Perawatan Tanggul Desa Tegalsari Kec.Widang Kab. Tuban. *MATAPPA: Jurnal Pengabdian Kepada Masyarakat*, *1*(2), 1-6.

Arends, R. (2012). *Learning to teach*. New York: McGraw-Hill.

Brunner, J. and Lewis, D. (2006). Planning for Emergencies. *Principal leadership*. April 2006. 6; 8 : p. 65-66.

Bandura, A. (1977). Self-efficacy: Toward unifying theory of behavioral change. *Psychological Review*, *84*(2), 191-215.

Batdi, V. (2014). The effects of problem based learning approach on students' attitude levels: A meta-analysis. *Educational Research and Reviews*, *9*(9), 272-276.

Bembenutty, H., Cleary, T., & Kitsantas, A., (2013). Applications of self-regulated learning applied across diverse disciplines: A tribute to Barry J. Zimmerman. Charlotte, NC: Information Age Publishing.

Eggen, P. D. & Kauchak, D. P. (2013). *Educational psychology:* Windows on clasrooms (9th edition). New Jersey: Pearson.

Daud, R, Sari, S. A., Milfayetty, S., & Dirhamsyah, M. (2014). PENERAPAN PELATIHAN SIAGA BENCANA, *1*(1), 26-34.

Gregory, E., Hardiman, M., Yarmolinskaya, J., Rinne, L., & Limb, C. (2013). Building creative thinking in the classroom: From research to practice. *International Journal of Educational Research, 62*, 43-50.

Havwina, T., Maryani, E., & Nandi (2016). Pengaruh pengalaman bencana terhadapkesiapsiagaan peserta didik dalam menghadapi ancaman gempabumi dan tsunami. *Jurnal Pendidikan Geografi*, *16*(2).

Ibrahim, M. (2012). *Pembelajaran berdasarkan masalah*. Surabaya: Unesa University Press.

Imafuku, R., Kataoka, R., Mayahara, M., Suzuki, H., & Saiki, T. (2014). Students' experiences in interdisciplinary problem-based learning: A discourse analysis of group interaction. *Interdisciplinary Journal of Problem-based Learning*, *8*(2), 1-19.

Jones, B. D., Epler, C. M., Mokri, P., Bryant, L. H., & Paretti, M. C. (2013). The effects of a collaborative problem-based learning experience on students' motivation in engineering capstone courses. *Interdisciplinary Journal of Problem-Based Learnin*g, *7* (2).

Jones, H. M. B. & Vall, O. C. (2014). Preparing special educators for collaboration in the classroom: Pre service teachers' beliefs and perspectives. *International Journal of Special Education*, *29*(1), 1-12.

Keller, M. J. (2010). *Motivational Design for Learning and Performance the ARCS Model Approach*. USA: Springer.

Khairudin, dkk. Dampak Pelatihan Pengurangan Risiko Bencana terhadap Kesiapsiagaan Komunitas Sekolah. *Prosiding Seminar Hasil Penelitian Kebencanaan TDMRC-Un syiah, Banda Aceh, 13-19 April 2011*. Banda Aceh: Universitas Syiah Kuala.

Lenawida. 2011. *PengaruhPengetahuan, Sikap, danDukunganAnggotaKeluargaTerhadapKesiapsiagaanRumahTanggadalamMenghadapi BencanaGempaBumi di DesaDeyah Raya KecamatanSyiah Kuala Kota Banda Aceh.* TesisUniversitasNegeri Medan.

Madlazim, Rahmadiarti, F., Masriyah,Indana, S., Sunarti, T., Prahani, B.K. (2020). An OrSAEv learning model to improve the disaster preparedness of STEM teacher candidates. *World Transactions on Engineering and Technology Education* 18 (2), pp.231.

Madlazim, and Supriyono (2014). Improving experiment design skills: Using the Joko Tingkir program as a learning tool of Tsunami topic. *Science of Tsunami Hazards* 33 (2) ,pp.133.

Moleong, L. J. 2007. *Metodologi Penelitian Kualitatif*. Bandung: Rosda.

Moreno, R. (2010). *Educational Psychology*. New York: Jhon Wiley & Sonc, Inc.

Munro. *Penyuluhan (Conseling) Suatu pendekatan Berdasarkan Keterampilan*, Ghalia Indonesia, Jakarta : 1983.

OECD. (2013). *PISA 2015 Collaborative Problem Solving Framework*. New York: OECD Publishing.

Paripurno, E. T., Munadi, K., Kusuma, S., Ismail, N., & Mardiatmo, D. (2019). Pembelajaran kebencanaan untuk mahasiswa di perguruan tinggi.

Pratiwi, E. & Prihatiningsih, D. (2016). Pengaruh Pelatihan Penanggulangan Bencana Gempa Bumi Terhadap Kesiapsiagaan Palang Merah Remaja (PMR) SMAN 1 Pleret Bantul Dalam Menghadapi Bencana. (Tesis) Universitas 'Aisyiyah Yogyakarta

Pribadi, K. dan Yuliawati, A. K. 2009. Pendidikan Siaga Bencana Gempa Bumi Sebagai Upaya Meningkatkan Keselamatan Siswa (Studi Kasus pada SDN Cirateun dan SDN Padasuka 2 Kabupaten Bandung). *Jurnal PendidikanTahun 9 Nomor 9*, Oktober 2009.

Slavin, E. R. (2011). *Educational psychology: Theory and practice.* Boston: Pearson.

Stalker, S. L., Cullen, T., & Kloesel, K. (2014). Using PBM to prepare educators and emergency managers to plan for severe weather. *Interdisciplinary Journal of Problem-Based Learning*.

Sugiyono. 2013. *Metode Penelitian Pendidikan Pendekatan Kuantitatif, Kualitatif, dan R&D.* Bandung: ALFABETA.

Temel, S. (2014). The effects of problems based learning on pre service teacher's critical thinking dispositions and perceptions of problems solving ability. *South African Journal of Education*, *34*(1), 1-20.

Trianto. 2010. *Model Pembelajaran Inovatif Berorientasi Konstrutivistik.* Surabaya: Pustaka Ilmu.

Utami, T.N. & Meutia Nanda, M. (2018). Pengaruh pelatihan bencana dan keselamatan kerja terhadap respons persepsi mahasiswa prodi ilmu kesehatan masyarakat. *Jurnal JUMANTIK*, *4*(1), 84-100.

Wademan, M.R. (2005). *Utilizing development research to guide people-capability maturity model adoption considerations.* Doctoral dissertation. Syracuse: Syracuse University. Dissertation Abstracts International, 67-01A, 434. (UMI No. 3205587)
9(2), 1-9.

Zimmerman, B. J. & Schunk, D. H. (2008). Motivation: An essential dimension of self-regulated learning. In D. H. Schunk & B. J. Zimmerman (Eds.), Motivation and self-regulated learning: Theory, research, and applications (pp. 1–30). Mahwah, NJ: Lawrence Erlbaum Associates.

ISSN 8755-6839

SCIENCE OF **TSUNAMI HAZARDS**

Journal of Tsunami Society International

Volume 39 **Number 3** **2020**

MECHANISM OF SEAWALL DESTRUCTION DUE TO TSUNAMI

Redha F. Inabah[1], Warniyati[1,2], David.S.V.L. Bangguna[3], Kuswandi[4], Djoko Legono[1], Nur Yuwono[1], Radianta Triatmadja[1,*]

[1]Department of Civil and Environmental Engineering, Universitas Gadjah Mada, Indonesia.
[2]Department of Civil Engineering, Engineering Faculty, Universitas Pattimura, Ambon, Indonesia
[3]Department of Civil Engineering, Universitas Sintuwo Maroso, Poso, Indonesia.
[4]Department of Civil and Planning Engineering, Institut Teknologi Medan, Medan, Indonesia.
[*]Corresponding author: radianta@ugm.ac.id

ABSTRACT

Tsunami that happened along Sunda Strait on 22 December 2018 was generated by the collapse of the flank of Anak Krakatau volcano in Indonesia. The tsunami hit Lampung and Sunda beaches areas. The hydrodynamic force of the tsunami hit everything on its course severely including seawalls that are used to protect the beach from erosion due to wind waves. The stability of such structure is limited to the design wind wave force. Tsunami has a significantly different nature compare to wind waves. When tsunami arrives at the coastline it becomes surge where, the water particle movement is significantly faster than that of the wind waves. The force of such high speed of water particles at a seawall may destroy and drag away the material far from the original location. Field survey was conducted following the tsunami event along Sunda Strait in Banten area. Based on the survey, a hydraulic simulation of seawall destruction due to tsunami was carried out in the laboratory. It was found that there were two distinct mechanisms of seawall destruction. When the land support of the seawall is relatively weak, the seawall may be dragged landward. However, when the land support behind the seawall is relatively strong, for example more than 40% of the seawall's total height that stabilize the seawall against the turning moment, the seawall may be dragged seaward by the tsunami return flow (run down). These mechanisms are relevant to tsunami mitigation. Consideration of seawall collapse due to return flow of tsunami should be taken into account since, normally tsunami is a wave train that attacks the beach in a series.

Keywords: *Tsunami, Seawall, Ruins, Mechanism, Physical Model*

1. INTRODUCTION

On 22 December 2018, a tsunami stroked Sunda Strait both along the Banten and Lampung coastal areas of Indonesia. The tsunami was induced by the collapse of the flank of Anak Krakatau Volcano (BMKG, 2018). It was a unique tsunami generation since no significant tremor was recorded prior to the tsunami event. Anak Krakatau erupted on 21 December 2018 and was followed by the second eruption on 22 December 2018 (BMKG, 2018). The volcano eruption was followed by a collapse of the flank into the sea which triggered the tsunami (BMKG, 2018). The location of Anak Krakatau Volcano is presented in Figure 1. A numerical simulation was conducted by (Giachetti et al., 2012). They reported that the slides caused an initial tsunami of 43 m.

The tsunami caused various damages along the coastal areas surrounding the Sunda Strait. Based on post tsunami survey, the heights and damage patterns in Lampung and Banten coastal areas significantly varied (Takabatake et al., 2019). Such variations could have been caused by the bathymetry, position and size of slides, and times of slides occurrence. So far, the surveys that were carried out along the affected areas was focused on tsunami height, inundation and run up. Information and discussion about the effect of the tsunami especially related to seawall and debris has not been reported so far. As occurred in the Aceh tsunami in 2004 and the East Japan tsunami in 2011, many types of debris can be devastating to other buildings and people. In order to mitigate tsunami disaster therefore, the debris and its effect should be minimized. One type of the debris during East Japan tsunami in 2011 is the ruin of seawalls. The destructions were due to the excessive forces of tsunami and scouring behind the seawall (Mikami, et al., 2012; Suppasri et al., 2013; Yeh, et al., 2013; Jayaratne, et al., 2016). Even a strong seawall such as that in Japan could be destroyed. The damaged seawalls have become debris and were drifted away from their original positions. The drifting of debris toward the land is unwanted as it may endanger other buildings or people.

In Indonesia, there is no seawall that was specially built to mitigate tsunami. Normally, seawalls in Indonesia are aimed at protecting the coastal area from erosion. This type of seawall is not designed to withstand the force of tsunami. Hence, it is expected that this type of seawall along the Sunda Strait would be destroyed due to the Sunda Strait tsunami. In order to understand the effect of tsunami on some of the seawall along the coast of Banten (Sunda Strait) a survey was conducted after the tsunami event. The survey was aimed to investigate the damage of structures in the land areas due to the hydrodynamic force of tsunami. Destruction on buildings was also the main concern.

This paper reported a survey on the Sunda tsunami destruction especially regarding the seawalls. Two different conditions of seawall destruction were found during the survey. These were a seawall at Batu Hideung beach and a seawall at Cherry beach. A simple laboratory experiment was carried out to explain the mechanism of seawalls destruction at these two locations.

Figure 1. Sunda Strait and Anak Krakatau Mountain (map from Google Earth image)

2. SURVEY AND EXPERIMENTAL WORKS

2.1 The Field Survey

The field survey was conducted six days after the tsunami event, starting from 28th of December to 31st December 2018. It was expected that after 5 days of the tsunami event, the survey could be conducted more easily whilst most of the destruction and debris have not been removed from their original positions. The survey was conducted at the location where the damage of structures has not been cleared out and where the destruction was still tractable. The survey locations were Kelapa Jangkung Beach, Sukarame Beach, Chery Beach, and Batu Hideung Beach. These areas are tourist destination beaches which are depicted in Figure 2.

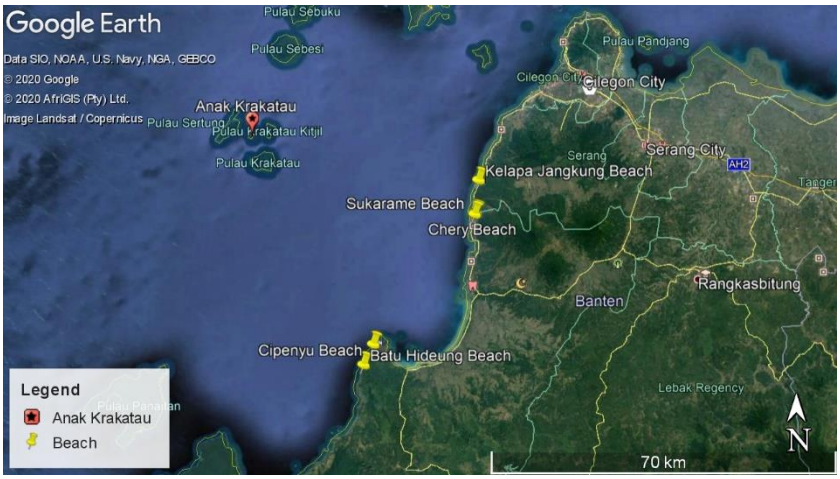

Figure 2. Survey locations in Banten Area (map from Google Earth Image)

2.1.1 The type of debris and the destruction

At Kelapa Jangkung beach, it can be seen that coconut tree debris has caused the building near the coast suffered from destruction. Figure 3 suggests that a rooftop was ruined by the debris. At that location the tsunami inundation was less than the roof height, hence the roof of the first-floor must have been ruined by floating debris. The coconut tree that could still be found in front of the building is the most possibly caused of the destruction. In Figure 4, many debris were found in the building adjacent to the building shown in Figure 3. On the right, a brick wall seems to be in a good condition or stable. The car on the background was seriously damaged. Probably the car has been swept by tsunami as debris and hit the building behind it. As can be seen, the car's body was deformed.

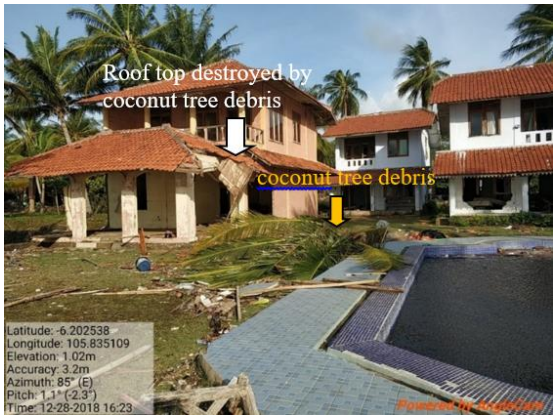

Figure 3. The rooftop of the building was damaged by a coconut tree debris

Figure 4. Debris in front of the building

A steel framework warehouse at Sukarame Beach was hit by tsunami as depicted in Figure 5. The lower part of the enclosure that was made of thin steel sheet was destroyed. The warehouse contained a number of agricultural equipment and machineries such as tractors that were for sales. When tsunami hit the building, all the equipment was washed away as debris and probably has caused further destruction to the enclosure. Some of the equipment was found approximately 150 m from the warehouse. Since there was no building behind the warehouse the debris could have rolled freely into the agricultural area. The debris indicated the strength of the tsunami in this area. Another indicator that demonstrated the strength of tsunami at this location is the fact that a building of brick wall with reinforce concrete frame was completely demolished. The wall with reinforce concrete was much more brittle when compare with the steel building. The ruins have become debris where some of them were drifted landward by tsunami. Approximately 300 m to the south from the warehouse location was a small container hotel location. The hotel was under construction where the containers were prepared near the beach. The containers were swept by tsunami as debris and stopped by trees along the road Figure 6.

Figure 5. The damage warehouse (steel frame, thin sheet steel enclosure) and brick wall with reinforce concrete frame buildings

Some of those containers have been installed on top of a stall foundation approximately 60 cm above the land surface. Figure 7 shows the condition of such container building. The tsunami force swept those containers land ward and luckily many of them were stopped by trees.

Figure 6. Container structure dragged by the tsunami

Figure 7. Survived container building

In the survey area, a seawall was destroyed almost completely as shown by Figure 8. A big boulder can be found on top of the ruined. These boulders could have originally been in front of the seawall (sea side) and were drifted by tsunami and finally hit the seawall. The boulder could have added more destruction to the seawall. In different location a very large boulder (3 m in diameter) was also found in land (Figure 9). The boulder could have been drifted tenth of meters from its original position in the beach. This justify that large boulder can be drifted far away by the Sunda Strait tsunami.

Figure 8. Boulders on top of the seawall in Batu Hideung Beach

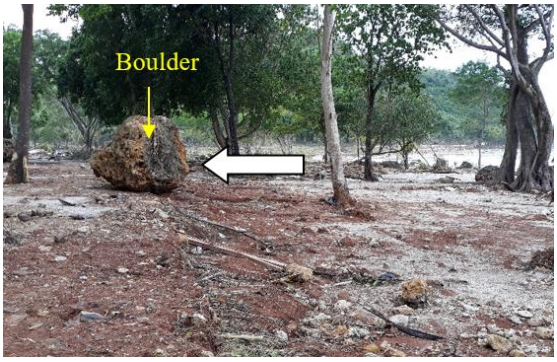

Figure 9. Boulder was dragged on land

2.1.2 Seawall destruction

Along the Chery Beach location, a relatively long seawall was constructed, probably to protect the beach from erosion. The seawall was not very strong as it was only made of cemented stones. The seawall was almost completely destroyed by the tsunami. An example of the ruins is given in Figure 10. As can be seen in the figure that, no part of the wall survived (Figure 10(a)). The dotted line represents the approximate original location of the seawall. In fact, some of the ruins were swept and drifted away as debris. This type of debris is also very dangerous for people during the tsunami event where they tried to escape from tsunami. Some of the debris was drifted approximately 50 m away from the beach (Figure 10(b)). Tsunami inundation at this location is about 3 m judging from the marks left by tsunami and dried leave of the coconut tree.

Another seawall in different location which is at Batu Hideung Beach (Figure 11) was also destroyed. This was a relatively new seawall construction. Similarly, the seawall was aimed at protecting the beach area from erosion. The depth of the foundations of both the Chery Beach and Batu Hideung are approximately 0.5 m.

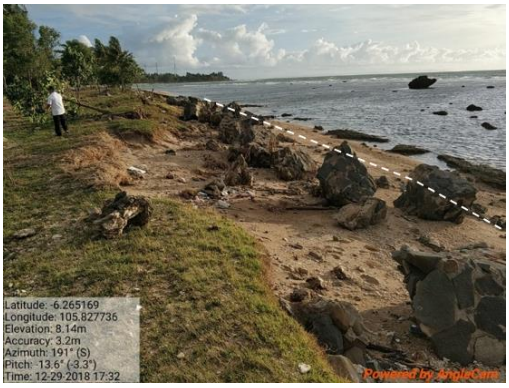

(a)

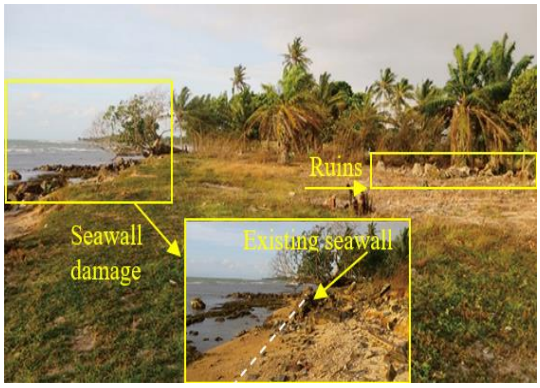

(b)

Figure 10. Seawall damage in Chery Beach Banten

Figure 11. Seawall damaged at Batu Hideung Beach Banten

Unlike the debris of seawall at Chery Beach, the ruins of Batu Hideung seawall were scattered at the seaside. There could have been a number of possibilities. First, the seawall was strong enough to withstand tsunami during run up due to the land support but, it was failed during the rundown time as no land support at the seaside. Second, there was a possibility that the area behind the seawall was inundated due to tsunami coming from adjacent location since the tsunami height along Sunda Strait varied considerably. For example, the inundation at Sukarame Beach were approximately 2 to 3 meters, however at TPI Sukanegara (fish auction) which is only 660 m to the north, there was almost no inundation on land. A witness whose house is near the fish auction explained that he could only saw that, the water of the river mouth (used as fishing boat harbor) was turbulence and that the boats were hitting each other very hardly. He confirmed that there was no significant inundation at that location. The rundown of the tsunami was probably the one that destroyed the seawall. This analysis is also supported by the fact that there is a hill at 120 m to 200 m (Figure 13) behind the seawall that could have reflected back the tsunami, increased the inundation depth behind the seawall and dragged the seawall and the ruins to the sea side. During the survey, the positions of the ruins were documented. The schematic positions of the original seawall and the ruins are given in Figure 12. The cross-section was measured along the original seawall position at every 4 m distance. The location of the seawall and the surrounding area are presented in Figure 13.

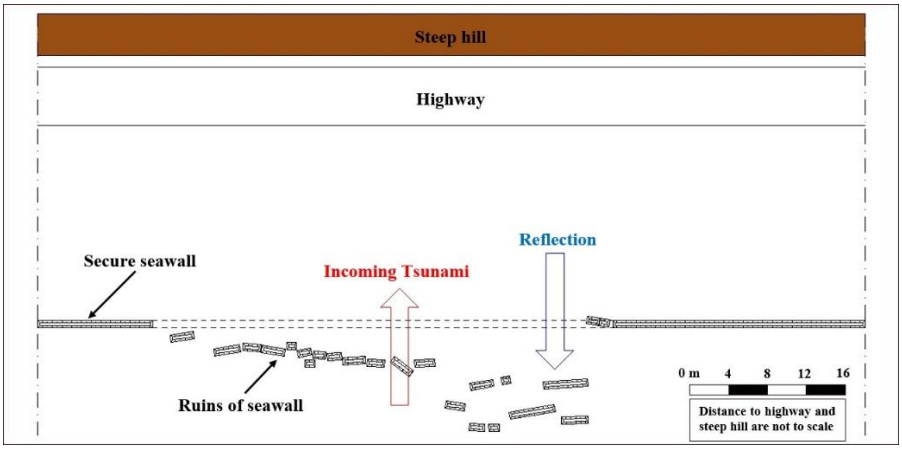

Figure 12. Schematic of seawall and ruins positions

Figure 13. Seawall position and the surrounding area (map from Google Earth Image)

As can be seen in Figure 12, the ruins of seawalls were found in front of the seawall original position at the beach side. It indicates that the debris were dragged seaward during tsunami run-down. In Figure 12, it can be seen that the debris were scattered with the longest distance of the debris from its original position was approximately 10 m. Actually, this is the preferred condition for a ruined seawall since, the dragging of debris seaward is expected not to harm anyone or buildings in the sea. Since seawalls are normally built along the coast to protect the beach from erosion, it is important to understand the failure mechanism which dictates the direction of the debris when the seawall is destroyed by tsunami.

2.2 Simulation of seawall destruction mechanism

A laboratory experiment was conducted to investigate the mechanism of seawall damage by the tsunami along Sunda Strait at Banten. The experiment was conducted at Gadjah Mada University, Indonesia. The tsunami surge was simulated based on dam break model. Such model has been used by many such as (Triatmadja and Nurhasanah 2012, Triatmadja and Benazir 2014). The validity of such method to simulate tsunami surge was discussed by (Kuswandi and Triatmadja 2019). The flume that was used for the simulation was 0.6 m wide, 0.4 m deep, 12 m long which was equipped with a quick release mechanism to generate tsunami surge. Water level probes were installed along the flume. A set of cemented seawall model was installed in and perpendicular to the flume. A block of the cemented seawall was modeled or represented by an acrylic of 0.06 m high, 0.016 m wide at the bottom and 0.015 m wide at the top. The seawall model scale was 1:20. The length of each element was 0.05 m. Each element can be placed next to the other elements to form a 0.60 m of seawall model perpendicular to the flume. The connection between seawalls can be strengthened using wedges. The wedges lengths can be varied to simulate the strength of the seawall to be modeled. The tsunami flume with tsunami generation (dam break) facility is presented in Figure 14. The scheme of seawall model test is given in Figure 15.

Figure 14. The flume equipped with dam break generation facility

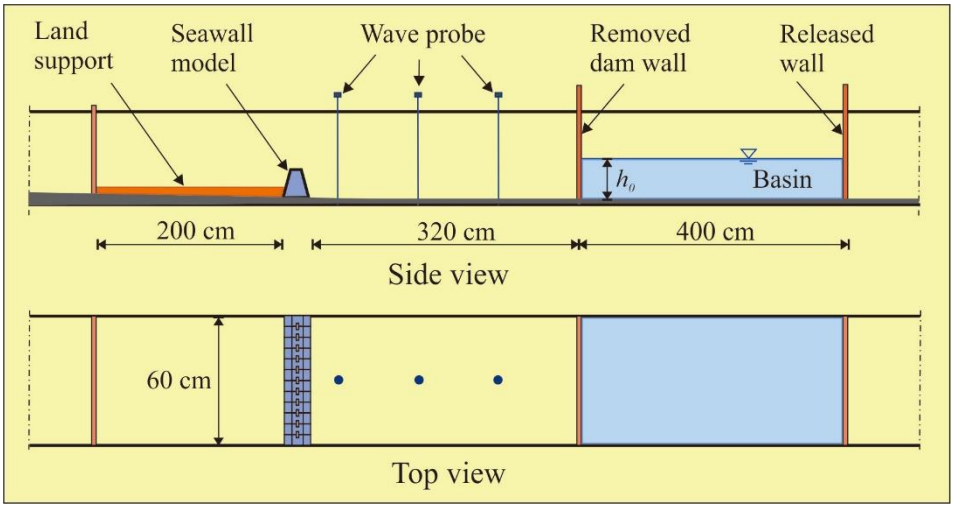

Figure.15. Schematic of seawall model test

Based on the field condition, a seawall model was set as follows. The seawall model was set perpendicular to the flume. At the boundary (flume walls) the seawall was fixed to simulate the undestroyed part in the field. In order to simulate the strength of the seawall, the wedges that connected the seawall was varied. These were 0.0 m (without wedge), 0.014 m, 0.021 m, and 0.028 m long. After the seawall was set, tsunami surge was generated from the upstream by lifting the gate that separate the flume into two parts. The upstream part was the basin that represent the source of tsunami. As the gate was lifted, the water in the basin surged toward the seawall model. The water depth of the basin was varied to create various tsunami inundation depths and forces on the seawall model.

3. RESULTS AND DISCUSSION

Prior to the hydrodynamic simulation, the seawall (cemented seawall) model strength was observed. This was conducted by a pull-out experiment that was aimed to observe the seawall model's strength under uniform static force. The sketches of the pull-out test are presented in Figure 16. The wedges that linked between two loose seawall element models are shown as small brown rectangles. The results of the loading tests for various wedge lengths are presented in Table 1.

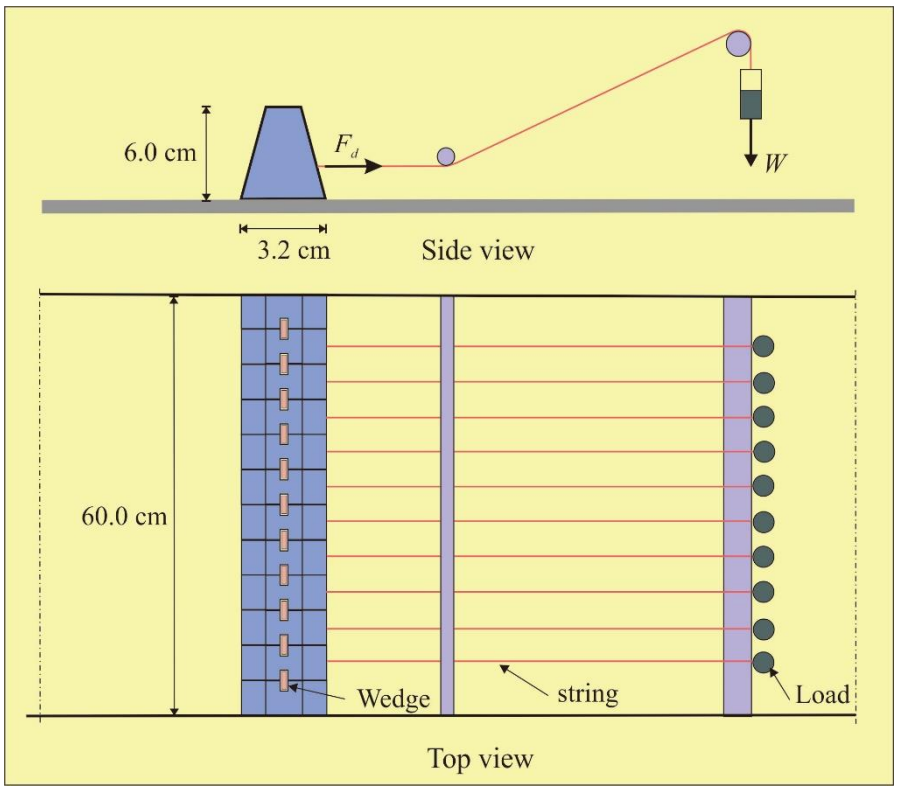

Figure 16. Schematic of pull out test

Table 1. Maximum (failure) loads of various wedge lengths

Wedge Length (cm)	Load at failure (N)
0	16.1
1.4	27.2
2.1	30.0
2.8	Not available

The strengths of the seawalls as described in Table 1 are not scaled to the real strength of the seawall however, they are needed to indicate the hydrodynamic force of the surge as they failed to withstand the tsunami force. This is because it is not possible to measure such force in the experiment using load cell since the seawall model should be kept fixed in place while the deformation may occur prior to the collapse. Computation of tsunami force based on Equation 1 may not bring a correct answer because, in reality the tsunami will overtop and overflow the seawall and hence the calculated force will be significantly higher than in reality. Using Table 1, the tsunami surge force on the seawall can be approximated based on the maximum load.

The experiment of the tsunami attack on seawall structure is presented in Figure 17. The first model was tested where the model was placed on top of the flume bed and no land support behind the wall. In this case, the seawall under the test would finally be damaged and was dragged landward. As can be seen in Figure 18, the broken seawall was dragged landward. The second model was tested where the seawall was supported by land of approximately 40% of the wall height (0.024 m). As indicated in Figure 19, the seawall was stable against the incoming tsunami. However, during run down, the seawall was destroyed and the debris was dragged seaward. Figure 19 shows the conditions of the seawall model after tsunami attack where the surge depth was 3.1 cm. It was the return flow or the run down that destroy the seawall. Hence the debris was dragged into the sea.

Tsunami force on the seawall model could be computed by equation proposed by (Triatmadja and Nurhasanah 2012) and presented as Equation (1).

$$F = C_f \, \rho(1 - n^2) B h U^2 \tag{1}$$

where C_f is a coefficient equals 1.03, ρ is the density of water, n is the ratio of the opening to the total area, B is the width of the building, h is the surge front depth and U is the front celerity ($U = 2\sqrt{gh}$).

The seawall conditions with no land support after tsunami attack are presented in Table 2. The ratio between the forces that destroy the seawall (calculated based on Equation 1) and the maximum load during pull-out tests are given in Table 2. It can be seen that the ratio varies from 0.78 to 1.45 when the seawall was destroyed. This indicates that Equation 1 may sometime slightly under predict or over predict the force. One of the reasons is that the tsunami, in this case, overtopped the model where Equation (1) is no longer valid.

(a) The tsunami hit the seawall

(b) The seawall was damaged by tsunami

Figure17. Simulation of seawall destruction due to tsunami

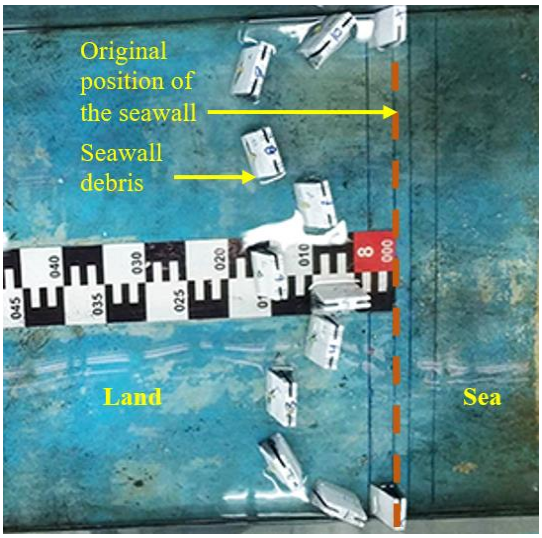

Figure 18. Debris of seawall were dragged landward, no land support behind the seawall

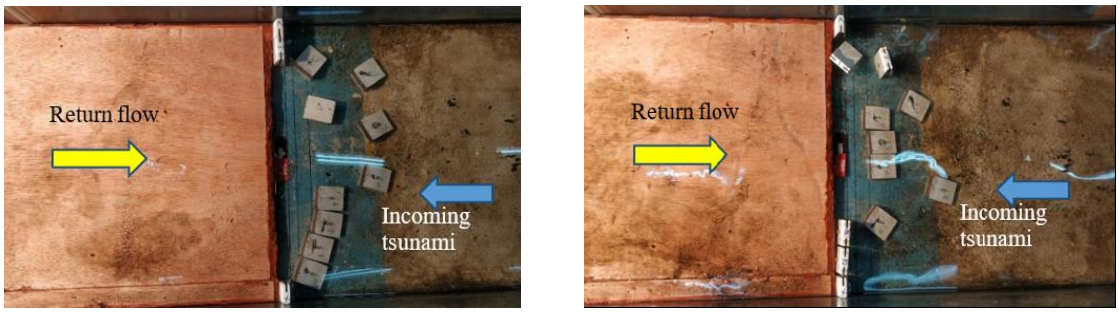

(a) Without wedges (b) With wedges of 1.4 cm

Figure 19. Seawall condition after wave attack (with land support)

Table 2. The seawall conditions under tsunami attack, no land support behind the seawall

Wedge length (cm)	Surge front height					
	1.9 cm		2.8 cm		3.1 cm	
	Final Condition	(Calculated force)/ (Maximum pull out force)	Final Condition	(Calculated force)/ (Maximum pull out force)	Final Condition	(Calculated force)/ (Maximum pull out force)
0	Secured	0.54	73% damaged	1.18	90% damaged	1.45
1.4	Secured	0.32	Bending and 47% damaged	0.7	80% damaged	0.86
2.1	Secured	0.29	Bending and 40% damage	0.63	70% damaged	0.78
2.8	Secured	-	bended (max.=7 cm)	-	bended (max.=7 cm)	-

Pull-out force creates almost total damage

4. CONCLUSION

Seawalls that are designed to protect the beach from erosion may not be able to withstand tsunami force. The destruction of the seawall can be caused by hydrodynamic force as well as impact force of boulder or debris material that hit the seawall during tsunami attack. Seawall debris as a result of tsunami attack may endanger other buildings and people. The direction of the seawall debris depends on whether it was the run-up or the run-down hydrodynamic force that destroy the seawall.

Based on the laboratory experiment, Equation 1 produced forces in the range between 70% to 150% of the maximum force that destroy the seawall. Sufficient land support behind the seawall, in our case approximately 40% of the seawall height, may held the seawall in place and avoid the destruction during run up. However, such seawall may be destroyed by the hydrodynamic force during tsunami run-down.

These mechanisms of destruction that determine the direction of the seawall debris are relevant to tsunami mitigation. Possible tsunami return flow (run down) is important for consideration since, normally tsunami is a wave train that attacks the beach in a series.

ACKNOWLEDGMENTS

The authors would like to thank the Department of Civil and Environmental Engineering for financing the survey. Our gratitude also goes to the Hydraulics and Hydrology Laboratory of The Center for Engineering Science Universitas Gadjah Mada that has supported the hydraulics simulation. The help of Mr. Kuwatono who manufactured the seawall model is highly appreciated.

REFERENCES

BMKG. 2018. "BMKG Ungkap Kronologi Tsunami Selat Sunda." *BMKG*.

Giachetti, T., Paris, R., Kelfoun, K., and Ontowirjo B. 2012. "Tsunami Hazard Related to a Flank Collapse of Anak Krakatau Volcano, Sunda Strait, Indonesia." *Geological Society, London, Special Publications 2012* 361:79–90.

Jayaratne, M. P. R., Premaratne, B., and Adewale, A. 2016. "Failure Mechanisms and Local Scour at Coastal Structures Induced by Tsunami." *Coastal Engineering Journal* 58(4).

Kuswandi and Triatmadja, R. 2019. "The Use of Dam Break Model to Simulate Tsunami Run-up and Scouring Around a Vertical Cylinder." *Journal of Applied Fluid Mechanics* 12(5):1395–1406.

Mikami, T., Shibayama, T. and Esteban, M. 2012. "Filed Survey of The 2011 Tohoku Earthquake and Tsunami in Miyagi and Fukusima Prefectures." *Coastal Engoneering Jpournal* 54(1).

Suppasri, A. Shuto, N., Imamura, F., Koshimura, S., Mas, E., Yalciner, A. C .2013. "Lessons Learned from the 2011 Great East Japan Tsunami: Performance of Tsunami Countermeasures, Coastal Buildings, and Tsunami Evacuation in Japan." *Pure and Applied Geophysics* 170(6–8):993–1018.

Takabatake, T et al. 2019. "Field Survey and Evacuation Behaviour during the 2018 Sunda Strait Tsunami." *Coastal Engineering Journal* 61(4):423–43.

Triatmadja, R. and Nurhasanah, A. 2012. “Tsunami Force On Buildings With Openings And Protection.” 6(4):1–17.

Triatmadja, R. and Benazier., 2014. “Simulation of Tsunami Force on Tows of Buildings In Aceh Region After Tsunami Disaster In 2004”, Journal of Science of Tsunami Hazard, Volume 33, Number 3, Page 156-169.

Yeh, H., Sato, S., and Tajima, Y. 2013. “The 11 March 2011 East Japan Earthquake and Tsunami: Tsunami Effects on Coastal Infrastructure and Buildings.” *Pure and Applied Geophysics* 170(6–8):1019–31.

ISSN 8755-6839

SCIENCE OF **TSUNAMI HAZARDS**

Journal of Tsunami Society International

Volume 39 **Number 3** **2020**

DEVELOPMENT OF EARTHQUAKE AND TSUNAMI EARLY WARNING APPLICATION BASED ON ANDROID

Madlazim[1], Supriyanto Rohadi[2], Soerja Koesuma[3], Ella Meilianda[4]

e-mail:madlazim@unesa.ac.id

[1] State University of Surabaya, Surabaya 60213, Indonesia
[2]Meteorology Climatology and Geophysics Council, DKI Jakarta 10720, Indonesia
[3]Sebelas Maret University, Solo 57126, Indonesia
[4] Syiah Kuala University, Aceh 23111, Indonesia

ABSTRACT

Ease of accessing and using earthquake and tsunami early warning applications is a priority in this study. It is related to the more time the community prepares for disaster mitigation. The purpose of this research is to produce an Android-based earthquake and tsunami early warning application. The availability of this fast android-based earthquake and tsunami early warning application can help in quicker and more reliable earthquake and tsunami early warning for short distances to areas that have the potential to impact a tsunami. The research method used in this research is the ADDIE development method (Analysis, Design, Development, Implementation, and Evaluation. In the first year, the focus of the development of the Rapid Tsunami Early Warning Application about 4 minutes after O.T. Our previous research results, which have supported many events this application will make it easier for us to complete the prototype target. The prototype of the Android-based earthquake and Tsunami, early warning application, has been tested in real-time at the Faculty of Mathematics and Natural Sciences, Surabaya State University, Indonesia. The results of the trial have shown the eligibility requirements.

Keywords: *Earthquake and tsunami early warning application; android; earthquake; Tsunami*

Vol 39 No. 2, page 183 (2020)

1. INTRODUCTION

The most destructive Tsunami is at proximity to areas that have a tsunami impact (for example, < 1000km) from the epicenter of the earthquake, arriving within 20-30 minutes after the time the earthquake occurred (O.T.). Effective early warning at this distance requires notification in less than 10 minutes after O.T. (e.g., Tsushima et al., 2011; Newman et al., 2011; Madlazim, 2011). At present, rapid assessment of potential tsunamis from earthquakes by organizations such as the Meteorology, Climatology and Geophysics Agency (BMKG), Japan Meteorological Agency (JMA), tsunami early warning system of the German-Indonesian tsunami warning system (GITEWS) or the West Coast and Alaska (WCATWC) and Pacific (PTWC) depends mainly on the initial estimate of the location of the earthquake, the depth and moment, M0, or the corresponding moment magnitude, Mw. However, reliable Mw calculations for large earthquakes are usually provided by CMT by the strength of the moment tensor, Mw, (Extröm et al., 2005), which requires waveform inversion, varying with rupture depth, earth models and other factors, and new available 20-30 min or more after an earthquake occurred (Hayes et al., 2011; Duputel et al., 2011). So a fast magnitude estimator such as Mwp has been used for Tsunami CMT warnings, but Mwp performs poorly compared to Mw and other discriminants for tsunami potential (Lomax and Michelini, 2011A, LM2011; Madlazim, 2011).

To produce effective and efficient earthquake and tsunami early warnings, especially for short distances to areas potentially affected by tsunamis, we use the method of calculating tsunami parameters quickly. We have provided a direct procedure for measuring tsunami parameters rapidly and accurately. (Lomax and Michelini, 2009B; LM2011; Lomax and Michelini, 2011B; Madlazim, 2011; Madlazim, 2013; Madlazim et al., 2019). Measuring steps for tsunami parameters use a direct procedure that is to measure tsunami parameters from P-wave seismogram data, the dominant period Td, duration more than 50 minutes, T50Ex, rupture duration, T0. T0 for large earthquakes is mainly related to the length of the rupture, L, and both Td and T0 will increase, then the depth of rupture, z, decreases, because the effects of shear modulus and rupture speed, V_r are reduced. We have shown that the product of the multiplication duration of Td x T0 or Td x T50Ex provides more information about the impact of tsunamis than discriminating against Mw, Mwp, Mwpd (Lomax and Michelini, 2009A, LM2009A; Madlazim, 2011; Madlazim, 2013; Madlazim et al., 2019), and other discriminants that are currently used. These results indicate that the tsunami potential is not directly related to the L x W x D product of the "seismic" fault model. As assumed by the use of the Mw discriminant so far and suggests otherwise that information about the length and depth can better explain the tsunami potential from the earthquake earth. Information about the length and depth of the rupture is provided by Td x T0 and Td x T50Ex, where explicit estimates of the length and depth of the rupture are complicated and cannot be determined quickly.

The Android-based earthquake and tsunami early warning system are still undergoing development to get a more practical, more accurate, and faster earthquake and tsunami early warning system. Powerful earthquake and tsunami early warning for

coastlines at a geographical distance (> 500 km) from the epicenter of the earthquake that caused the Tsunami requires notification within 15 minutes of the origin time of the quake. More recently, through the analysis of P wave (30º-90º, GCD) teleseismic seismograms, Lomax and Michelini (2009) have shown that high frequency, rupture duration, T0, greater than about 50 or T0 more top 65 (Madlazim, 2011; Madlazim, 2013 Madlazim et al., 2015) strengthens the accuracy of Tsunami early warning. Lomax and Michelini (2009) exploited this result through the direct "duration-exceedance" (D.E.) procedure applied to seismograms on GCD 10º-30º to determine quickly whether T0 for earthquakes tends to exceed 50-55 s and thus become potentially Tsunami tsunamis. Madlazim et al. (2015) implemented the Lomax and Michelini (2009) teleseismic methods to measure T0 and T50Ex (D.E.) with a threshold of 65 seconds for T0, 1 for T50Ex and 10 seconds for dominant periods (Td).

The problem in this research is how the development of earthquake and tsunami early warning applications based on android for Indonesia and surrounding areas? To develop this application, we certainly need a valid, fast, and accurate earthquake and tsunami early warning application that we have previously developed (Madlazim et al., 2019).

2. METHODS

To achieve the objectives of this study, the ADDIE model was used (Aldoobie, 2015), which consisted of 5 stages; Analysis, Design, Develop, Implementation, and Evaluation Phase. The first stage is the Analysis phase. After this stage is completed, the results are evaluated. The second stage is the design stage. After this stage is complete, the results are evaluated. The third stage is the Develop stage. After this stage is completed, the results are evaluated. The fourth stage is the Implementation stage. After this stage is completed, the results are evaluated. The fifth stage is the Evaluation stage. This Evaluation Phase is carried out for all stages.

The five stages in the ADDIE model are as follows: 1. ***Analysis Stage***; The main activity is analyzing the need for developing an Android-based earthquake and tsunami early warning application and examining the appropriateness and requirements of the application development. The problem of accuracy and speed of the implementation of earthquake and tsunami early warning that has been applied is no longer relevant to the needs of targets, technology, and availability of real-time seismogram data. 2. ***Design Stage***. At the design stage, it is an activity to design an Android-based earthquake and Tsunami early warning application development. The design of this application is still conceptual and will underlie the next development process. 3. ***Development Stage***. At the Development stage contains the activities of product design realization. Compiled conceptual framework for the application of the development of an Android-based earthquake and tsunami early warning application and realized into a product that is ready to be implemented. For example, at the design stage, the app has been designed, which is still conceptual, so at the development stage, the application is made with the device so that

it is ready to be implemented. 4. ***Implementation Stage***. At this stage, the Android-based earthquake and Tsunami early warning application development is implemented in real and relevant situations, and initial evaluation is carried out to provide feedback on subsequent applications. Real-time data used to estimate earthquake and tsunami parameters are taken from data recorded by a network of local seismic stations managed by GEOFON. The process of implementing the determination of tsunami parameters uses the Jokotingkir software (Madlazim, Prastowo, and Hardy 2015). 5. ***Evaluation Stage***. At this evaluation, the stage is carried out at the process stage and the end of the activity. At the end of each stage, an evaluation is carried out, and at the end of the activity, the previous 4 stages are also evaluated. Revisions are made according to the evaluation results or needs that cannot be fulfilled by the application. The steps for developing an Android-based earthquake and tsunami early warning application are presented in the flowchart of Figure 1.

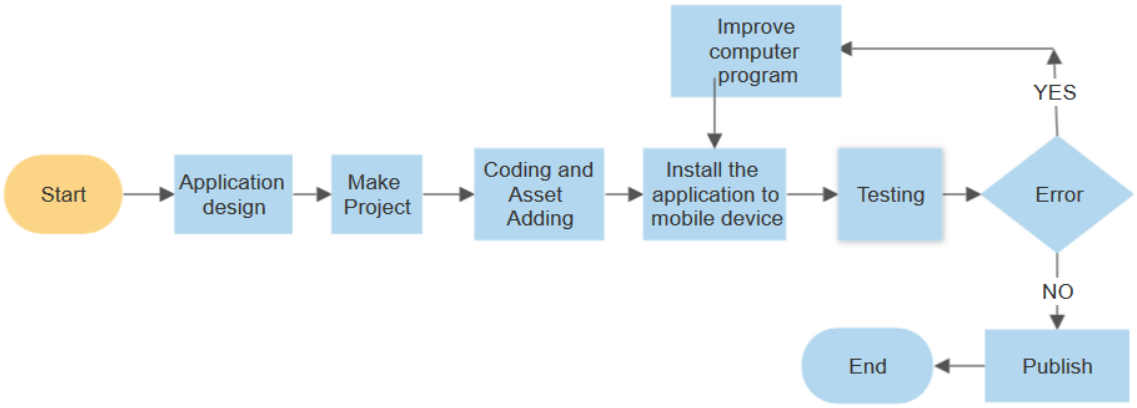

Figure 1. *Flowchart of Android-based earthquake and tsunami early warning application development.*

The application design referred to in Figure 1 above is a tsunami early warning application about 4 minutes after the web-based origin time (O.T.) earthquake that has been developed by Madlazim et al. (2019). The development of an Android-based earthquake and tsunami early warning application is a previous continuation of research.

3. RESULTS AND DISCUSSION

The results of this Android-based earthquake and Tsunami early warning application development can be divided into 2, the results of which are the development of an android-based earthquake and tsunami early warning application presented in Fig. 2. This application can be accessed downloaded and installed from the play store with Jotingkir tsunami prediction keywords or can also be directly accessed from the following website https://play.google.com/store/apps/details?id=com.smadia.prediksi_tsunami_jokotingkir.

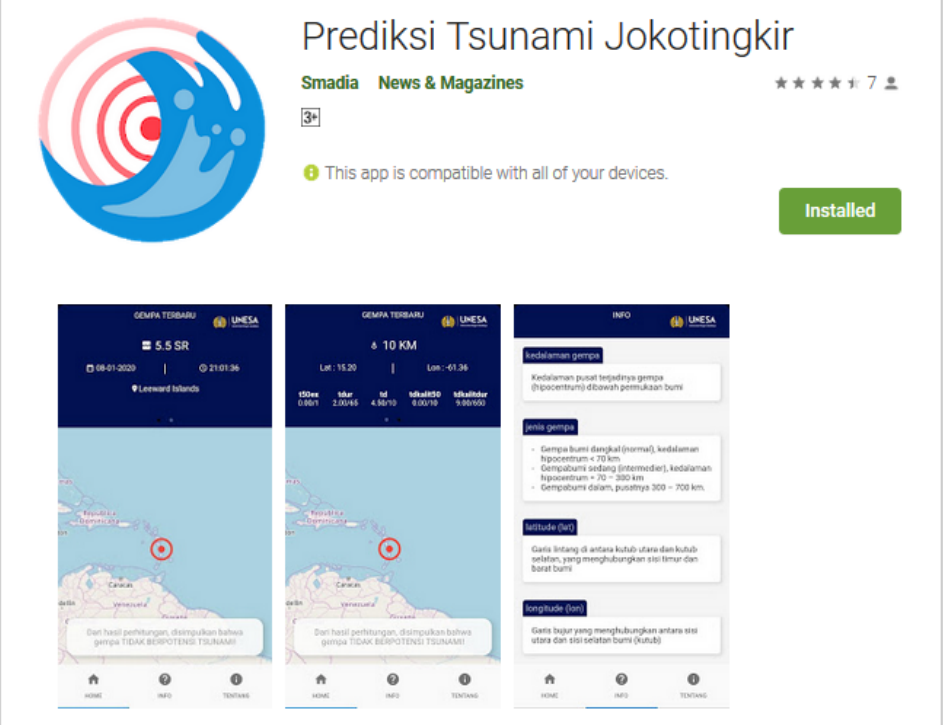

Figure 2. Android-based earthquake and tsunami early warning application.

Example of an Android-based earthquake and tsunami early warning application output as shown in Fig. 3.

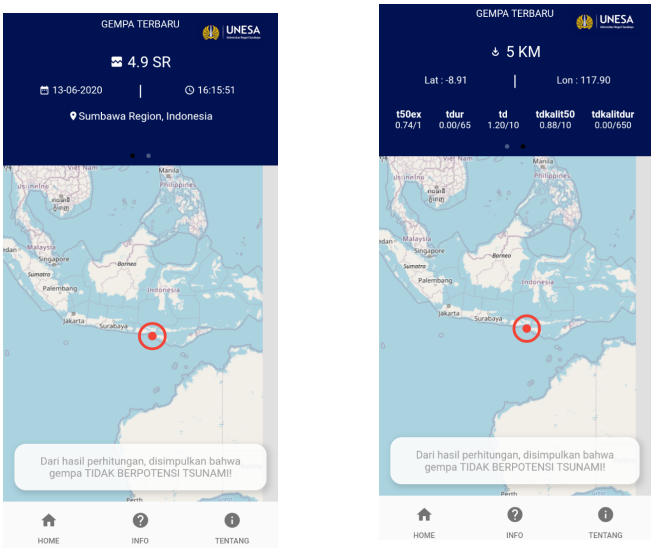

Figure 3. Example of an Android-based earthquake and tsunami early warning application output for an earthquake that occurred in the Sumbawa region, Indonesia, on June 13, 2020.

In the android-based earthquake and tsunami early warning applicatio n, as shown in Figure 2 and Figure 3, there are two pages. On the first page, there is information on earthquake magnitude, earthquake time and date, location of the region, and earthquake epicenter indicated by red dots and circles on the map. This can make it easier for users when and where an earthquake occurs and information on whether an earthquake has a potential tsunami or cannot also be read on page one or page two. Especially for Tsunami early warning, if an earthquake has a tsunami potential, then the writing of the tsunami potential that is below the map will turn red. The application icon also appears notification. On page two that can be seen by sliding the screen to the left then there will be information about the depth of latitude and longitude earthquakes and tsunami parameters (duration 50 exceed = T50ex, earthquake duration = Tdur, dominant period = Td, Tdur and T50Ex multiplication and multiplication Td and T50Ex) in numeric form. How these tsunami parameters are measured has been explained by Lomax and Michelini (2012), Madlazim et al. (2015), and Madlazim and Tjipto Prastowo (2019). On page two there is also map information and earthquake epicenter as well as information on tsunami potential or not as shown on page one. This information is made two pages with the aim that information is clear and not complicated. Based on the results of the application for the 478 most recent earthquakes used for testing the Android-based earthquake and tsunami early warning application that occurred in Indonesia and now from May 12, 2019, to June 15, 2020, with the magnitude of the earthquakes ranging from 4 to 7.5 as shown in Figure 4 and Figure 5. Of the 478 earthquakes, there were 477 earthquakes, which predicted the tsunami warning was right and there was only one earthquake that had an early warning that the Tsunami had a false warning. This application program has been improved so that in the future, it is expected that there will be no more false warnings.

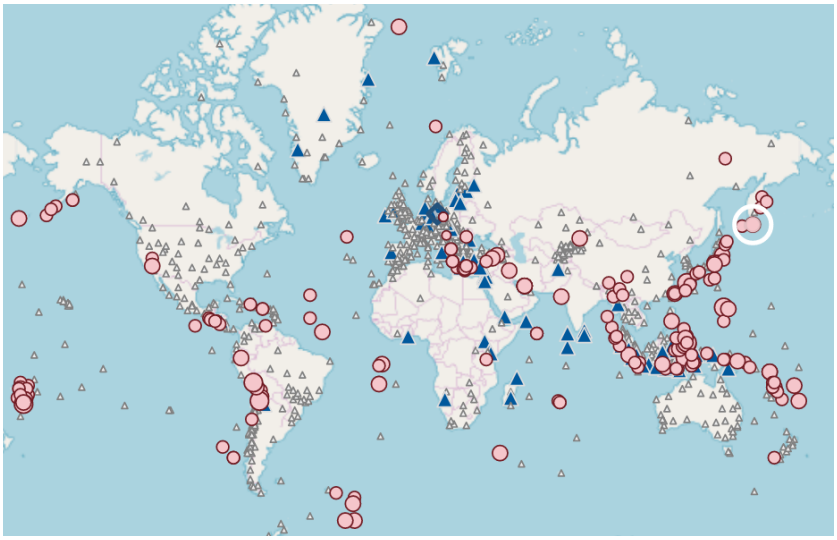

Figure 4. Attributes of the G.E. seismic network (GEOFON) that blue triangles and other than the G.E. network (small triangles) earthquake epicenter map that occurred from May 12, 2020, to June 15, 2020, which is used for testing Android-based earthquake and tsunami early warning applications.

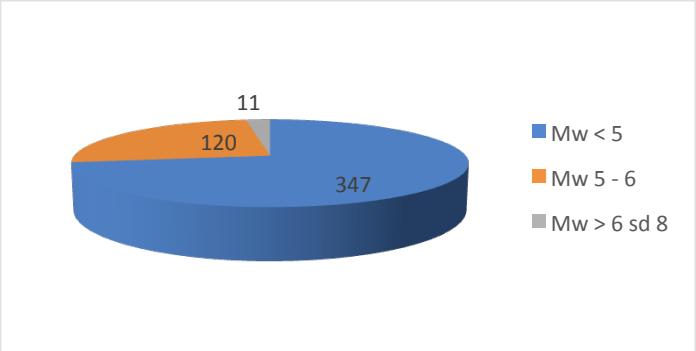

Figure 5. The magnitude of earthquakes that occurred in Indonesia and surrounding areas from May 12, 2020, to June 15, 2020, which is used for testing Android-based earthquake and tsunami early warning applications

4. CONCLUSION

Android-based earthquake and tsunami early warning applications have been developed and tested in real time using 478 earthquakes that occurred in Indonesia and its surroundings from May 12, 2020, to June 15, 20220. The results of the trials show that the application of earthquake and tsunami early warning This Android-based meets eligibility.

ACKNOWLEDGMENTS

Thanks to GEOFON for licensing the use of seismic stations and earthquake data in real-time. Thanks to DRPM of Ministry of Research, Technology and Higher Education of the Republic of Indonesia that support this research under grant number B/11645/UN38.9/LK.04.00/2020.

REFERENCES

Aldoobie, N. (2015). ADDIE Model Analysis phase. *American International Journal of Contemporary Research*, *5*(6), 68–72.

Duputel, Z., Rivera, L., Kanamori, H., Hayes, G.P., Hirshorn, B., and Weinstein, S. (2011), Real-time W phase inversion during the 2011 off the Pacific coast of Tohoku Earthquake, *Earth Planets Space*, 63(7), 535-539.

Ekström, G., Dziewonski, A.M., Maternovskaya, N.N., and Nettles, M. (2005), Global seismicity of 2003: Centroid-moment-tensor solutions for 1087 earthquakes, *Phys. Earth Planet. Inter.*, *148*, 327– 351.

Lomax, A., Michelini, A. and Piatanesi, A. (2007), An energy-duration procedure for rapid determination of earthquake magnitude and tsunamigenic potential, *Geophys. J. Int.*, *170*, 1195-1209, doi:10.1111/j.1365-246X.2007.03469.x

Lomax, A. and Michelini, A. (2009A), *M*wpd: A duration-amplitude procedure for rapid determination of earthquake magnitude and tsunamigenic potential from *P* waveforms, *Geophys. J. Int.*, *176*, 200–214, doi:10.1111/j.1365-246X.2008.03974.x

Lomax, A. and Michelini, A. (2009B), Tsunami early warning using earthquake rupture duration, *Geophys. Res. Lett.*, *36*, L09306, doi:10.1029/2009GL037223

Lomax, A. and Michelini, A. (2011A), Tsunami early warning using earthquake rupture duration and *P*-wave dominant period: the importance of length and depth of faulting, *Geophys. J. Int.*, *185*, 283–291, doi: 10.1111/j.1365-246X.2010.04916.x

Lomax, A. and Michelini, A. (2011B), Erratum, *Geophys. J. Int.*, *186*, 1454, doi:

10.1111/j.1365-246X.2011.05128.x

Lomax, A. and Michelini, A. (2012), Tsunami Early Warning Within Five Minutes. Pure and Applied Geophysics, Volume 170, Issue 9–10, pp 1385–1395.

Madlazim. 2011. "Toward Indonesian Tsunami Early Warning System by Using Rapid Rupture Duration Calculation,." *SCIENCE OF TSUNAMI HAZARDS*.

Madlazim, M., Tjipto Prastowo, and Thomas Hardy. 2015. "Validation of Joko Tingkir Software Using Tsunami Importance." *Science of Tsunami Hazards*.

Madlazim. 2011. "Toward Indonesian Tsunami Early Warning System by Using Rapid Rupture Duration Calculation,." *SCIENCE OF TSUNAMI HAZARDS*.

Madlazim, M., Tjipto Prastowo, and Thomas Hardy. 2015. "Validation of Joko Tingkir Software Using Tsunami Importance." *Science of Tsunami Hazards*.

Madlazim, T. Prastowo, S. Rohadi, and T. Hardy. 2018. "Filter-M Application for Automatic Computation of P Wave Dominant Periods for Tsunami Early Warning." *Science of Tsunami Hazards*.

Madlazim, Supriyanto Rohadi, Soerja Koesoema, Ella Meilianda. 2019. Development Of Tsunami Early Warning Application Four Minutes After An Earthquake. *Science of Tsunami Hazards*, **38** (3), 132-141.

Madlazim and T. Prastowo. 2019. Beta testing for increased accuracy and improved performance of the Indonesian Tsunami early warning application (Ina-TEWA). *Science of Tsunami Hazards*, **38** (4), 16-178.

Tanioka, Yuichiro, and Kenji Satake. 1996. "Tsunami Generation by Horizontal Displacement of Ocean Bottom." *Geophysical Research Letters*.

Moore, G. F., Bangs, N. L., Taira, A., Kuramoto, S., Pangborn, E., Tobin, H. J. (2007), Three- Dimensional Splay Fault Geometry and Implications for Tsunami Generation. *Science* 318, 1128, DOI: 10.1126/science.1147195

Nakamura, Y. (1988), On the urgent earthquake detection and alarm system (UrEDAS), *Proc. of the 9th World Conference on Earthquake Engineering*, Tokyo-Kyoto, Japan.

Newman, A.V., and Okal, E.A. (1998), Teleseismic Estimates of Radiated Seismic Energy: The E/M_0 Discriminant for Tsunami Earthquakes, *J. Geophys. Res.*, **103** (11), 26,885- 98.

Newman, A.V., Hayes, G., Wei, Y., and Convers, J. (2011), The October 25 2010 Mentawai tsunami earthquake, from real-time discriminants, finite-fault rupture, and tsunami excitation, *Geophys. Res. Lett.*, *38*, L05302, doi:10.1029/2010GL046498.

Ozaki, T. (2011), Outline of the 2011 off the Pacific coast of Tohoku Earthquake (Mw 9.0) - Tsunami warnings/advisories and observations, *Earth Planets Space*, *63*, 827–830, doi:10.5047/eps.2011.06.029

Polet, J., and Kanamori, H. (2009), Tsunami Earthquakes, in *Encyclopedia of Complexity and Systems Science*, edited by A. Meyers, Springer, New York, 10370pp., doi:10.1007/978- 0-387-30440-3_567

PTWC (2009), Tsunami Bulletin Number 001, issued at 1830Z 19 MAR 2009, Pacific Tsunami Warning Center/NOAA/NWS.

Satake, K. (2002), Tsunamis, in *International Handbook of Earthquake and Engineering Seismology*, pp. 437–451, eds W.H.K. Lee, H. Kanamori, P.C. Jennings & C. Kisslinger, Academic Press, Amsterdam.

Tanioka, Yuichiro, and Kenji Satake. 1996. "Tsunami Generation by Horizontal Displacement of Ocean Bottom." *Geophysical Research Letters*.

Tsushima, H., Hirata, K., Hayashi, Y., Tanioka, Y., Kimura, K., Sakai, S., Shinohara, M., Kanazawa, T., Hino, R., and Maeda, K. (2011), Near-field tsunami forecasting using offshore tsunami data from the 2011 off the Pacific coast of Tohoku Earthquake, *Earth Planets Space*, *63*, 821–826.

ISSN 8755-6839

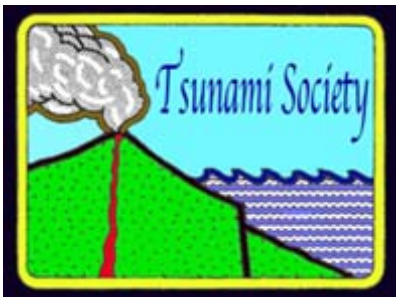

SCIENCE OF TSUNAMI HAZARD

Journal of Tsunami Society International

Volume 39 **Number 3** **2020**

WWW.TSUNAMISOCIETY.ORG

TSUNAMI SOCIETY INTERNATIONAL, 1741 Ala Moana Blvd. #70, Honolulu, HI 96815, USA.

WWW.TSUNAMISOCIETY.ORG